THE FLORIDA STATE UNIVERSITY

COLLEGE OF ARTS AND SCIENCES

A MULTI-LAYER MODEL OF COASTAL UPWELLING

By

RICHARD T. MCNIDER

A Thesis submitted to the
Department of Meteorology in
partial fulfillment of the
requirements for the degree of
Master of Science

Approved:

James J. O'Brien
Professor directing Thesis

Peter J. Sinnasch

Raymond O. Stuhlinger

Wyatt Howard

David Lopez

May, 1972

APPENDIX A

DERIVATION OF MODEL EQUATIONS

Consider the Navier-Stokes equations in the form

$$\frac{\partial u}{\partial t} + u\frac{\partial u}{\partial x} + v\frac{\partial u}{\partial y} + w\frac{\partial u}{\partial z} - fv = -\frac{1}{\rho}\frac{\partial p}{\partial x} + \frac{1}{\rho}\frac{\partial \tau^x}{\partial z} + A\left(\frac{\partial^2 u}{\partial x^2} + \frac{\partial^2 u}{\partial y^2}\right) \qquad (A\text{-}1)$$

$$\frac{\partial v}{\partial t} + u\frac{\partial v}{\partial x} + v\frac{\partial v}{\partial y} + w\frac{\partial v}{\partial z} + fu = -\frac{1}{\rho}\frac{\partial p}{\partial y} + \frac{1}{\rho}\frac{\partial \tau^y}{\partial z} + A\left(\frac{\partial^2 v}{\partial x^2} + \frac{\partial^2 v}{\partial y^2}\right) \qquad (A\text{-}2)$$

$$\frac{\partial p}{\partial z} = -\rho g \qquad \text{(hydrostatic assumption)} \qquad (A\text{-}3)$$

$$\frac{\partial u}{\partial x} + \frac{\partial v}{\partial y} + \frac{\partial w}{\partial z} = 0 \qquad (A\text{-}4)$$

To formulate our layered model we want to integrate (A-1), (A-2), and (A-4) over the depth of the layer. In performing the integration we assume the velocity components and density are independent of depth within the layer. We thus obtain

$$\frac{\partial u_j}{\partial t} + u_j\frac{\partial u_j}{\partial x} + v_j\frac{\partial v_j}{\partial y} - fv_j = -\frac{1}{\rho}\int_B^T \frac{\partial p}{\partial x}\,dz + \left(\tau_j^{Tx} - \tau_j^{Bx}\right)/\rho h_j + A\left(\frac{\partial^2 u_j}{\partial x^2} + \frac{\partial^2 u_j}{\partial y^2}\right) \qquad (A\text{-}5)$$

$$\frac{\partial v_j}{\partial t} + u_j\frac{\partial v_j}{\partial x} + v_j\frac{\partial v_j}{\partial x} + fu_j = -\frac{1}{\rho}\int_B^T \frac{\partial p}{\partial y}\,dz + \left(\tau_j^{Ty} - \tau_j^{By}\right)/\rho h_j + A\left(\frac{\partial^2 v_j}{\partial x^2} + \frac{\partial^2 v_j}{\partial y^2}\right) \qquad (A\text{-}6)$$

where m = number of layers $\qquad j = 1(1)m.$

If we invoke the hydrostatic assumption then the pressure within each layer can be written

$$\left.\begin{aligned} p_1 &= p_A + \rho_1 g \left[\sum_{j=0}^{m-1} h_{m-j} + D(x) - z\right] \\ p_2 &= p_A + \rho g h_1 + \rho_2 g \left[\sum_{j=0}^{m-2} h_{m-j} + D(x) - z\right] \end{aligned}\right\} \qquad (A\text{-}7)$$

and in general

$$p_k = p_A + \sum_{j=1}^{k-1} \rho_j g h_j + \rho_k g \left[\sum_{j=0}^{m-k} h_{m-j} + D(x) - z\right]$$

in which P_A is the air pressure and $D(x)$ is the height of the topography above $z = 0$.

Upon taking the horizontal derivatives and neglecting atmospheric pressure variations we find

$$\frac{\partial p_k}{\partial x} = \sum_{j=1}^{k-1} \rho_j g \frac{\partial h_j}{\partial x} + \rho_k g \left[\sum_{j=0}^{k} \frac{\partial h_{m-j}}{\partial x} + \frac{\partial D}{\partial x}\right] \qquad (A\text{-}8)$$

$$\frac{\partial p_k}{\partial y} = \sum_{j=1}^{k-1} \rho_j g \frac{h_j}{y} + \rho_k g \left[\sum_{j=0}^{k} \frac{\partial h_{m-j}}{\partial y}\right] \qquad (A\text{-}9)$$

If we perform the integration as indicated above, we obtain

$$\frac{1}{\rho_k} \int_B^T \frac{\partial p_k}{\partial x} = \frac{h_k}{\rho_k} \sum_{j=1}^{k-1} \rho_j \frac{\partial h_j}{\partial x} + h_k g \left[\sum_{j=0}^{m-k} \frac{\partial h_{m-j}}{\partial m} + \frac{\partial D}{\partial x}\right] \qquad (A\text{-}10)$$

The interior and bottom stress τ^T and τ^B can be formulated using energetic and dimensional considerations to yield

$$\tau^{Tx}_{j+1} = \tau^{Bx}_j = \rho C_I \bar{q} (u_j - u_{j+1}) \qquad (A\text{-}11)$$

and dimensional considerations to yield

$$\tau^{Tx}_{j+1} = \tau^{Bx}_j = \rho C_I \bar{q} (u_j - u_{j+1}) \qquad (A\text{-}11)$$

$$\tau^{Ty}_{j+1} = \tau^{By}_j = \rho C_I \bar{q} (v_j - v_{j+1}) \qquad (A\text{-}12)$$

in which $q_j = \left((u_j)^2 + (v_j)^2\right)^{1/2}$

$\bar{q} = (q_j + q_{j+1})/2$ (See O'Brien and Hurlburt, 1972)

The stress terms include the gain or loss of kinetic energy to a layer as well as dissipation of kinetic energy in the layer through velocity shear of the mean velocity between the layers.

Combining the terms from the analysis above we find

$$\frac{\partial u_j}{\partial t} + u_j \frac{\partial u_j}{\partial x} + v_j \frac{\partial u_j}{\partial y} = fv_j - g \sum_{i=1}^{n} \frac{\partial h_i}{\partial x} - g \frac{\partial D}{\partial x}$$

$$+ \sum_{i=1}^{j-1} \varepsilon_{ij} \frac{\partial h_i}{\partial x} + \left(\tau_j^{Tx} - \tau_j^{Bx}\right)/\rho h_j + A \left(\frac{\partial u^2}{\partial x^2} + \frac{\partial v^2}{\partial x^2}\right) \qquad \text{(A-13)}$$

$$\frac{\partial v_j}{\partial t} + u_j \frac{\partial v_j}{\partial x} + v_j \frac{\partial v_j}{\partial y} = fu_j - g \sum_{i=1}^{n} \frac{\partial h_i}{\partial y} - g \frac{\partial D}{\partial y}$$

$$+ g \sum_{i=1}^{j-1} \varepsilon_{ij} \frac{\partial h_i}{\partial y} + \left(\tau_j^{Ty} - \tau_j^{By}\right)/\rho h_j + A \left(\frac{\partial^2 v_j}{\partial x^2} + \frac{\partial^2 v_j}{\partial y^2}\right) \qquad \text{(A-14)}$$

If we integrate the continuity equation given in (A-4) vertically in the layer

$$\int_B^T \left[\frac{\partial u}{\partial x} + \frac{\partial v}{\partial y} + \frac{\partial w}{\partial z}\right] dz = 0 \qquad \text{(A-15)}$$

then

$$h_j \frac{\partial u_j}{\partial x} + h_j \frac{\partial v_j}{\partial y} dz + w(T) - w(B) = 0 \qquad \text{(A-16)}$$

We can note, however, that

$$w(T) = \frac{dh_j}{dt} + w(B) = \frac{\partial h_j}{\partial t} + u_j \frac{\partial h_j}{\partial x} + v_j \frac{\partial h_j}{\partial y} \qquad \text{(A-17)}$$

$$w(T) = \frac{dh_j}{dt} + w(B) = \frac{\partial h_j}{\partial t} + u_j \frac{\partial h_j}{\partial x} + v_j \frac{\partial h_j}{\partial y} \qquad \text{(A-17)}$$

so the continuity equation for each layer becomes

$$\frac{\partial h_j}{\partial t} = -\frac{\partial}{\partial x}(u_j h_j) - \frac{\partial}{\partial y}(v_j h_j) \qquad \text{(A-18)}$$

Thus, Eqs. (A-13), (A-14), and (A-18) form a complete layered set of equations. Boundary conditions suitable for the problem require horizontal velocities to vanish at the coast and at the computational boundary offshore. Layer thicknesses at the boundary are calculated from the continuity equation (A-18).

The above equations are integrated numerically using implicit methods for terms governing the internal and external gravity waves. Standard difference schemes are used in other terms such as centered-in time for Coriolis terms, quadratic averaging for the advective terms, and leap-frog for time differences.

APPENDIX B

GLOSSARY

baroclinic - the state of stratification in a fluid in which constant density surfaces intersect surfaces of constant pressure.

barotropic - the state of stratification in a fluid in which density is a function of pressure only; i.e., not baroclinic. A barotropic response indicates a response independent of depth.

cross gradient flow - the flow of fluid across lines of constant pressure. In a rotating system geostrophic flow is directed parallel to constant pressure lines thus cross gradient flow implies ageostrophic flow.

cross stream flow - the flow perpendicular to a main stream. Specifically in this paper, cross-stream flow is that flow perpendicular to the coast.

cyclonic - having a sense of rotation the same as that of the earth's rotation as viewed from above the local vertical. So that cyclonic means counterclockwise in the Northern Hemisphere, counterclockwise in the Northern Hemisphere, clockwise in the Southern Hemisphere, and is undefined at the equator.

downwarping - in the specific sense as used in this paper, downwarping refers to a lowering of an interface at the coast.

Ekman pumping - the imposition of negative vertical velocity due to a negative wind stress curl.

Expressed in the model by

$$-\frac{dh_1}{dt} = \frac{1}{f\rho}\frac{\partial}{\partial x}\tau^{sy}$$

where h_1 is the layer thickness and τ is the y-directed surface wind stress.

Ekman transport - non-geostrophic transports due to wind stress at the surface. Transports are directed at right angles to the stress and are given by

$$U_E = \tau^{sy}/f \; ; \quad V_E = -\tau^{sx}/f \; .$$

geostrophic balance - a balance between the horizontal Coriolis forces and the horizontal pressure forces. The balance results in flow parallel to lines of constant pressure and directed to the right of the pressure gradient in the Northern Hemisphere.

geostrophic adjustment - the mutual adjustments to geostrophic equilibrium of the mass and velocity fields when an imbalance exists.

when an imbalance exists.

internal gravity waves - a wave in fluid motion having its maximum amplitude within the fluid or at an internal boundary. The wave will move at a speed given by

$$c_{Ig} = \sqrt{g\varepsilon H_1}$$

where H_1 = depth of fluid to the interface

ε = density contrast across the interface

g = acceleration of gravity.

isopycnal - surface of constant density.

longshore - denotes a direction parallel to the coast. For the present study this indicates a direction along the y axis.

longshore pressure gradient - a pressure gradient parallel to the coast so that $\partial p/\partial y$ is non-zero.

longshore transport - the mass flux through a section perpendicular to the coast.

Rossby waves - low frequency waves which propagate westward relative to the basic current. Existence of the waves is based on conservation of absolute vorticity and variation of the Coriolis parameter with latitude. The speed of the waves is given by

$$c = U - \frac{\beta\lambda^2}{4\pi^2}$$

$$c = U - \frac{\beta\lambda^2}{4\pi^2}$$

where U is the speed of the basic current, λ is the wavelength, and $\beta = df/dy$.

semi-implicit numerical method - a scheme in which terms that govern the fastest moving waves are treated implicitly. Implicit schemes average terms which are not time differenced over a time interval that includes an unknown time level. Direct inversion of the matrix of coefficients or iteration methods are used to predict the variable at the new level.

sigma-t - an abbreviated value of the density of sea water given by

$$\sigma_t = [\rho(S,t) - 1] \times 10^3$$

where ρ is the value of the sea water density in cgs units.

subgeostrophic flow - cross gradient flow toward lower pressure in a rotating system.

supergeostrophic flow - cross gradient flow toward higher pressure in a rotating system.

Sverdrup balance - a simplified expression relating meridional transport to the wind-stress curl. A balance is considered between Coriolis force, pressure force, and the surface wind stress.

A vorticity equation is formed resulting in

$$\beta \int_{-\infty}^{0} \rho v \, dz = - \left(\frac{\partial \tau^{sx}}{\partial y} - \frac{\partial \tau^{sy}}{\partial x} \right)$$

$$\beta \int_{-\infty}^{0} \rho v \, dz = - \left(\frac{\partial \tau^{sx}}{\partial y} - \frac{\partial \tau^{sy}}{\partial x} \right)$$

where My is meridional transport.

thermohaline mixing - the diffusion of heat and salt.

transverse circulation - see cross-stream flow.

upwelling - the rising of water toward the surface from subsurface layers.

REFERENCES

REFERENCES

Blumsack, S., 1971: The transverse circulation near a coast. J. of Phys. Ocean., 2, 34-40.

Cahn, A., 1945: An investigation of the free oscillations of a simple current system. J. Meteor., 2, 113-119.

Chemical Rubber Company, 1964: Standard Mathematical Tables. Student Edition, Cleveland, 561 pp.

Compania Administradora del Guano, Departmento de Oceanografia e Ictologia, 1960: Mapas Mensuales del Litoral Peruano.

Defant, A., 1961: Physical Oceanography, Vol. II. Pergamon Press, London.

Ekman, V. W., 1905: On the influence of the earth's rotation on ocean currents. Arkiv. Mat. Astron. Fysik., 12, 1-52.

Hsueh, Y., and R. N. Kenny, III, 1971: Steady coastal upwelling in a continuously stratified ocean. J. of Phys. Ocean., 2, 27-33.

Hurlburt, H. E., and J. D. Thompson, 1972: Coastal upwelling on a β-plane. (Submitted to J. of Phys. Ocean.)

Kwizak, M., and A. Robert, 1971: A semi-implicit scheme for grid point atmospheric models of the primitive equations. Mon. Wea. Rev., 94, 32-36.

Mooers, C. N. K., 1970: The interaction of an internal tide with the frontal zone in coastal upwelling region. Ph.D. Dissertation, Oregon State University, Corvallis, Oregon, 480 pp.

Mooers, C. N. K., R. L. Smith, and C. A. Collins, 1972: The dynamic structure of the frontal zone in the coastal upwelling region off Oregon. (Submitted to J. of Phys. Ocean.)

O'Brien, J. J., and H. E. Hurlburt, 1972: A numerical model of coastal upwelling. J. of Phys. Ocean., 2, 14-26.

Rossby, C. -G., 1938: On the mutual adjustment of pressure and velocity distribution in certain simple current systems, II. J. of Mar. Res., 1, 239-263.

Rossby, C. -G., 1938: On the mutual adjustment of pressure and velocity distribution in certain simple current systems, II. J. of Mar. Res., 1, 239-263.

REFERENCES - Continued

Sielecki, A., and M. G. Wurtele, 1970: The numerical integration of the non-linear shallow-water equations with sloping boundaries. J. Comput. Phys., 6, 219-236.

Smith, R. L., 1968: Upwelling. Oceanographic Marine Biology, Annual Review, Vol. 6, London Geo. Allen and Unwin, Ltds., 11-47.

Stuart, W. D., 1971: Evaporite deposition in a layered sea: A wind driven dynamical model. Ph.D. Dissertation, Northwestern University, Evanston, Illinois.

Thompson, J. D., and J. J. O'Brien, 1972: Time-dependent coastal upwelling. (Submitted to J. of Phys. Ocean.)

Yoshida, K., 1967: Circulation in the eastern tropical oceans with special reference to upwelling and undercurrents. Japan J. Geophys. 4, No. 2, 1-75.

Yoshida, K., and H. L. Mao, 1957: A theory of upwelling of large horizontal extent. J. of Marine Res., 16, 40-54.

VITA

Mr. Richard T. McNider was born July 9, 1948, in Century, Florida. In 1970 he graduated Phi Beta Kappa from the University of Alabama with a B.S. in Mathematics. He began his graduate study in the Department of Meteorology at the Florida State University in September 1970.

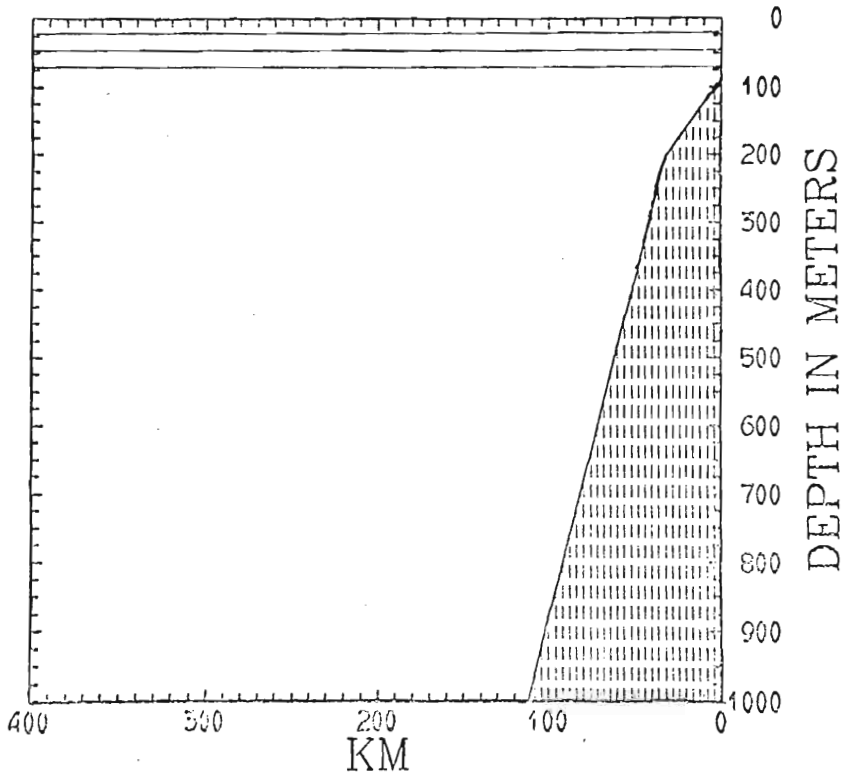

Fig. 13.-Model geometry and bottom topography for the Oregon coast simulation. Layer thicknesses are h_1 = 20 m, h_2 = 25 m, h_3 = 25 m, h_4 = 930 m. The stratification imposed is $\Delta\sigma_t$ 2.0, 0.5, 0.5.

confined entirely to the lower layer. Sielecki and Wurtele (1971) have shown that the equations can be integrated for a case in which an interface intersects the topography. This is accomplished by extrapolating in time to predict the position of an interface as it moves up the topography. Experiments employing this technique have been undertaken, however, results thus far have been unsatisfactory.

The wind stress used is constant at the coast (e.g., no curl, see Fig. 1). The model solutions for this case may be found in Fig. 14 with only the upper right hand corner of the model region depicted in the height profiles. Since the upper layer is only 20 m thick, the first interface surfaces after 4.5 days. The longshore velocity is equatorward in all four layers with a strong surface jet. No poleward undercurrent is observed. This is not in agreement with observations.

We can explain why a countercurrent fails to develop in this model. As we mentioned in a previous section, the poleward undercurrent forms in response to a breakdown of geostrophy in the onshore flow near the coast leading to subgeostrophic flow. In the present case we expect the countercurrent to form over the sharply sloping shelf. However, over the sloping shelf the fluid in the lowest layer is being accelerated in response to thinning of the layer by the topography. Thus instead of onshore subgeostrophic flow which yields a countercurrent we have a supergeostrophic flow which inhibits the formation of a countercurrent. This deficiency in the model could be eliminated by permitting the lower interfaces to intersect the topography and would allow a countercurrent
This deficiency in the model could be eliminated by permitting the lower interfaces to intersect the topography and would allow a countercurrent
to develop to the left of the shelf topography.

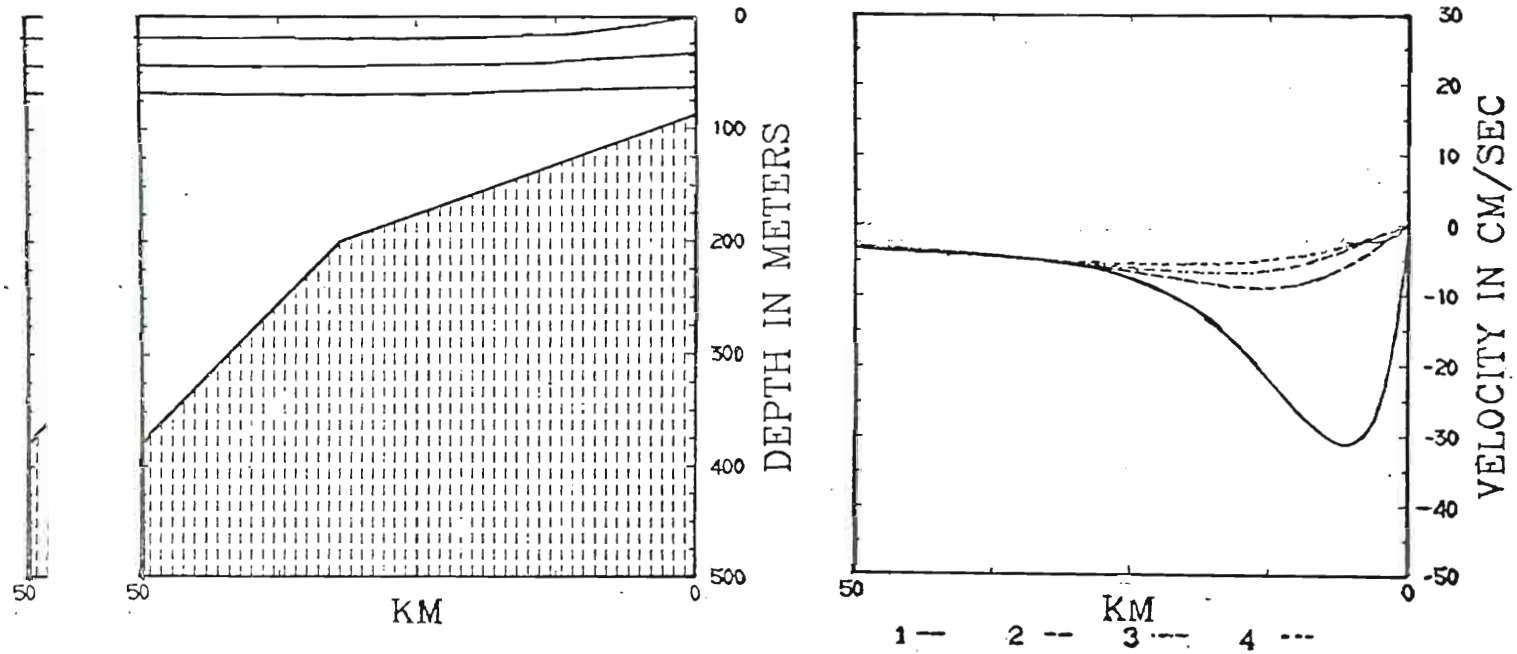

Fig. 14.-Height profiles (left) and velocity profiles (right) after 4.5 days for the Oregon coast simulation.

5. INTERNAL GRAVITY WAVES

We have shown that time dependent phenomena such as inertial oscillations and internal gravity waves are prominent features of the solutions. In this section we want to investigate the production and behavior of the propagating internal gravity waves in the model. The streamfunctions in Figs. 3, 4, 9, and 10 show that the internal waves are generated at the coast and slowly propagate out to sea. The waves decay rapidly as they move offshore and their apparent wavelength is appreciably shortened. The investigation of these waves is similar to the geostrophic adjustment problem discussed by Rossby (1938), Cahn (1945) and others.

The internal waves are excited and propagate along the first internal interface. Below this interface the waves are barotrophic and behave in accordance with continuity requirements. Let us consider the following simple linear model equations for a two-layer system

$$\frac{\partial u_1}{\partial t} = fv_1 - g\,(h_1 + h_2)_x \qquad (27)$$

$$\frac{\partial v_1}{\partial t} = -fu_1 + \tau^{sy}/\rho H_1 \qquad (28)$$

$$\frac{\partial u_2}{\partial t} = fv_2 - g\,(h_1 + h_2)_x + g\,\varepsilon_{12}\,h_{1x} \qquad (29)$$

$$\frac{\partial v_2}{\partial t} = -fu_2 \qquad (30)$$

$$\frac{\partial h_j}{\partial t} = -H_j \frac{\partial u_j}{\partial x} \qquad j = 1(1)2 \qquad (31)$$

$\partial t \quad - \quad - H_j \partial x \qquad j = 1(1)2$

where H_j is the initial layer thickness. Suppose we assume the flow is negligible in the lower layer (this can be justified by allowing $h_1 << h_2$

so that return flow supplying the upwelling motions is extremely small) then (29) becomes

$$g\,(h_1 + h_2)_x = g\,\varepsilon_{12}\,h_{1x} \tag{32}$$

It is also convenient to divide the velocity into a constant Ekman drift component and a perturbation component; e.g.,

$$u = \bar{u} + u' \qquad \text{where} \qquad \bar{u} = \tau^{sy}/f\,H_1 = u_E \tag{33}$$

Using (31) and (32) we can rewrite Eqs. (27), (28), (31) as

$$\frac{\partial u'}{\partial t} + g\,\varepsilon_{12}\,h_x = fv \tag{34}$$

$$\frac{\partial v}{\partial t} = -fu' \tag{35}$$

$$\frac{\partial h}{\partial t} + H_1\,\frac{\partial u'}{\partial t} = 0 \tag{36}$$

(the subscripts have been dropped).

The initial and boundary conditions are:

$$\begin{aligned} &u(0,t) = 0 && u'(x,0) = 0 \\ &\bar{u}(0,t) = u_E && v(x,0) = 0 \\ &u'(0,t) = -\tau^{sy}/fH_1 && h(x,0) = 0 \\ &u'(-\infty,t) = 0 \end{aligned} \tag{37}$$

If we eliminate variables in (34) - (36) in favor of u, we obtain

$$u'_{tt} - g\,\varepsilon_{12}\,H_1\,u'_{xx} + f^2 u' = 0 \tag{38}$$

with conditions

$$\begin{aligned} &u'(0,t) = -u_E && u'(x,0) = 0 \\ &u'(0,t) = 0 && \frac{\partial u'}{\partial t}(x,0) = 0 \\ &u'(0,t) = 0 && \frac{\partial u'}{\partial t}(x,0) = 0 \end{aligned}$$

We normalize the coordinates in (38) using

$$\alpha = -x\,(f/\sqrt{g\,\varepsilon_{12}\,H}) \text{ and } \eta = tf \tag{39}$$

to obtain

$$u'_{\eta\eta} + u' - u'_{\alpha\alpha} = 0 \tag{40}$$

Laplace transform methods allow us to find a solution to (40) in transform space of the form

$$U(\alpha,s) = -\frac{u_E}{s} e^{-(s^2+1)^{1/2}\alpha} \tag{41}$$

where s is the transform variable. The inverse transform to the above equation can be found in appropriate tables (CRC Standard Mathematical Tables, 1964)

$$u'(\alpha,\eta) = u_E \int_{\alpha}^{\eta} \frac{\alpha}{(\eta'^2 - \alpha^2)^{1/2}} J_1\left(\sqrt{\eta'^2 - \alpha^2}\right) d\eta' - u_E \tag{42}$$

with limits on the transformation

$$f(s) = e^{-\alpha s} - e^{-\alpha(s^2+1)^{1/2}} \Rightarrow F(\eta) = 0 \quad \text{for} \quad 0 < \eta < \alpha$$

$$f(s) = \frac{e^{-\alpha s}}{s} \Rightarrow F(\eta) = 0 \quad \text{for} \quad 0 < \eta < \alpha .$$

We cannot evaluate directly the integral found in (42). However, we can obtain an asymptotic expansion valid for $\eta > 1$ given by

$$u'(\alpha,\eta) = u_E\left[1 - e^{-\alpha} - \frac{\alpha}{\eta} J_0\left(\sqrt{\eta^2 - \alpha^2}\right) - \frac{\alpha}{\eta^3}\sqrt{\eta^2-\alpha^2}\, J_1\left(\sqrt{\eta^2 - \alpha^2}\right)\right.$$

$$\left. + \ldots\right) - u_E \tag{43}$$

where J_0 and J_1 are Bessel functions of the first kind.

To determine the behavior of the solution this expression was evaluated numerically in space and time. The results are shown in Fig. 15.

The solutions behave in a manner similar to those of Cahn (1945) 15.

The solutions behave in a manner similar to those of Cahn (1945) for a slightly different geometry. As in the model solutions the waves

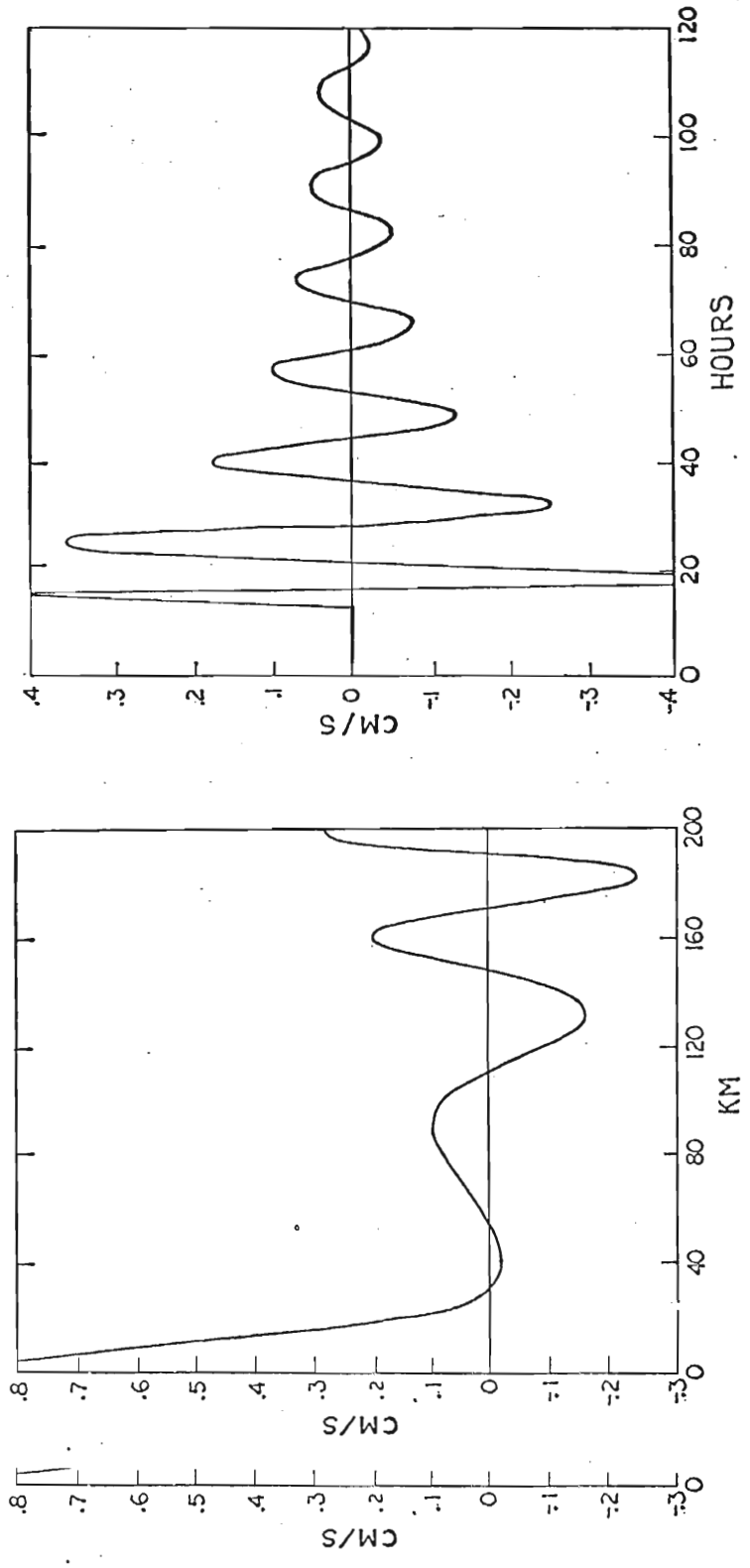

Fig. 15.-Perturbation velocities in the u field. Solutions (left) as a function of x after 48 hours. The coast is now on the left with several waves visible. The solutionsare also shown as a function of t (right) for a point 40 km from the coast. Strong damping of waves can be noted.

have a length of 40-60 km near the coast and the wavelength decreases offshore. If we took several snapshots of the solution in time we would find peaks forming near the coast. The peaks move offshore at the internal gravity wave speed ($\sqrt{g\,\varepsilon_{12}H_1}$) while the amplitude slowly decreases. Fig. 15 also gives the solution in time from which we see the wave period is approximately the inerial period. We also note that successive waves passing a point have increasingly smaller amplitudes. The damping is not due to friction (which we have completely neglected in the problem). Instead, the amplitude of the waves gradually becomes smaller as the energy of the oscillation excited by the impulsive start of the wind is radiated into a wider band of fluid.

The presence of internal gravity waves in the real ocean is well documented (Defant, 1961; Yoshida and Mao, 1957). In an upwelling zone because of the manner in which the waves are damped they may exert some type of cumulative effect. This effect may show up as a consistent downwelling region just outside the primary upwelling zone, however, this is only speculation. An understanding of the actual effects of the waves would require extensive momentum budget considerations which have not been made to date.

6. CRITIQUE

We have attempted to study some details of the vertical structure of the upwelling circulation. Certain points should be noted that have been neglected in our investigation.

A major drawback to the present model is that integration must cease when the upper interface reaches the sea surface. More realistically, we should allow the upper interface to behave as a surface front and investigate its behavior under the surface wind stress. Stuart (1971) for a circular basin has indicated one method which may be useful in implementing this scheme. A second problem (already mentioned) is the inability of the computer program to allow interfaces to intersect the sloping boundaries. These two problems are related in that both deal with cases in which the initial number of layers is reduced at some point in the model region.

Thermohaline mixing between layers has also been disregarded. We have thus implicitly assumed the time scale for interfacial mixing is greater than that for the vertical transport processes.

All model cases, so far, have dealt with the fluid initially at rest thus omitting all effects of the general ocean circulation. The geostrophic general circulation could be included by a judicious choice of interfacial and sea surface slopes in the model. Tidal interaction (Mooers, 1970) with the upwelling process should also be investigated.

7. SUMMARY

A four layer numerical model of a stratified ocean on a β-plane has been used to investigate the vertical structure of the wind driven upwelling circulation. Over a flat shelf the return flow supplying the upwelling motions is found to be evenly distributed throughout the lower three layers. The width of the upwelling zone spreads laterally with increasing depth and the strength of the vertical motion is reduced.

In the longshore flow an equatorward surface jet and a poleward undercurrent are the dominant features. The equatorward jet axis tilts offshore with depth. The depth at which the poleward undercurrent forms depends upon the stratification and wind stress imposed. Downwarping of the interfaces is noted in response to the poleward undercurrent. Propagating internal gravity waves excited at the coast by the impulsive start of the wind stress are trapped within 200 km of the coast.

In the second layer (23) we see the terms are of opposite sign thus we expect small velocities in this layer. However, a strong density contrast between layer 1 and 2 coupled with a widening of the upwelling zone with depth would predict equatorward flow near the edge of the upwelling zone and poleward flow near the coast. Fig. 3 for the four-layer model indicates this type of behavior in the second layer with equatorward flow at approximately 20 km and near zero velocity at the coast.

4.2 Flat shelf - wind stress curl at the coast

The model geometry for this case is the same as discussed previously with a flat shelf and layer thicknesses of 25, 25, 50 and 100 m. The problem has been changed, however, by introducing curl in the wind stress in the coastal region (see Fig. 7). The inclusion of the positive curl may more realistically depict the wind stress distribution by parameterizing the frictional effects of the adjacent land. Little actual wind data are available for upwelling regions with which to determine a realistic offshore stress profile. Some data from the Peruvian coast do indicate a positive curl in the wind stress (Compania Administradora del Guano Departmento de Oceanografie e Ictologia, 1960).

We will consider two different density profiles in this section but emphasize the effect of the new wind stress distribution.

The solutions, Fig. 8, are for the same $\Delta\sigma_t$ stratification as discussed earlier for the beta model: 2.0, 0.5, 0.5. Although the positive wind stress curl is more conducive to upwelling through Ekman suction, the actual upwelling at the coast is decreased. The decreased upwelling wind stress curl is more conducive to upwelling through Ekman suction, the actual upwelling at the coast is decreased. The decreased upwelling may be explained by the reduction of the one-sided divergence at the coast in accordance with the smaller wind stress at the boundary. The

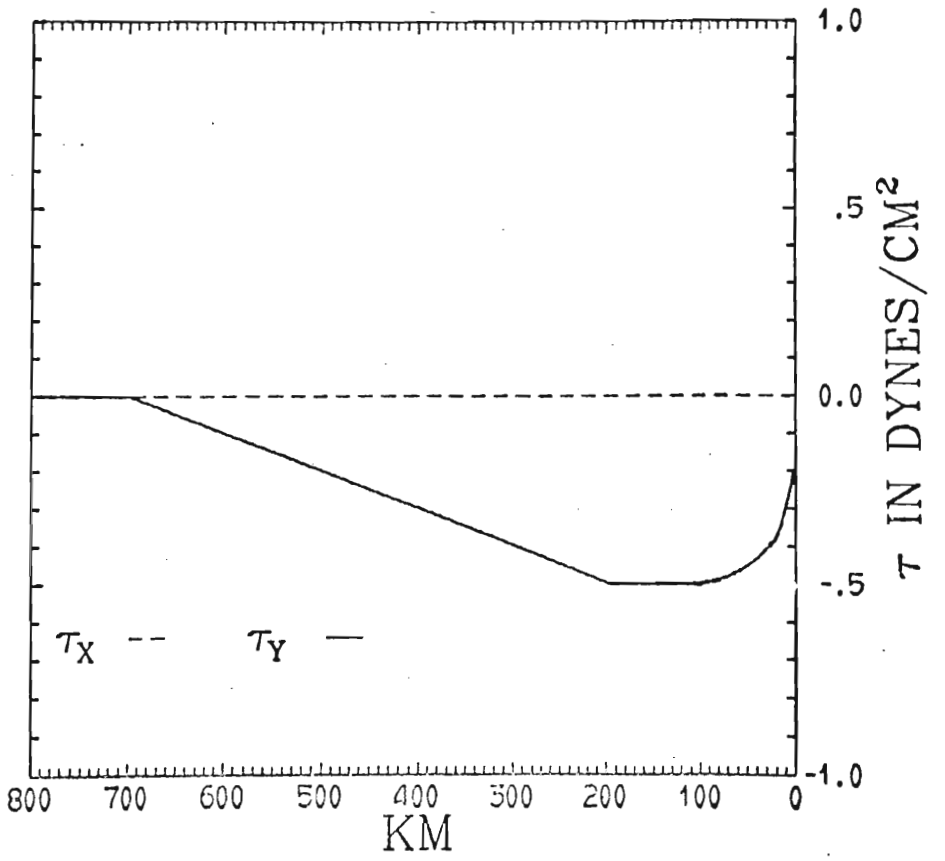

Fig. 7.-Wind stress components as a function of x with curl near the coast. τ_{sy} is shown by solid line and τ_{sx} is zero everywhere.

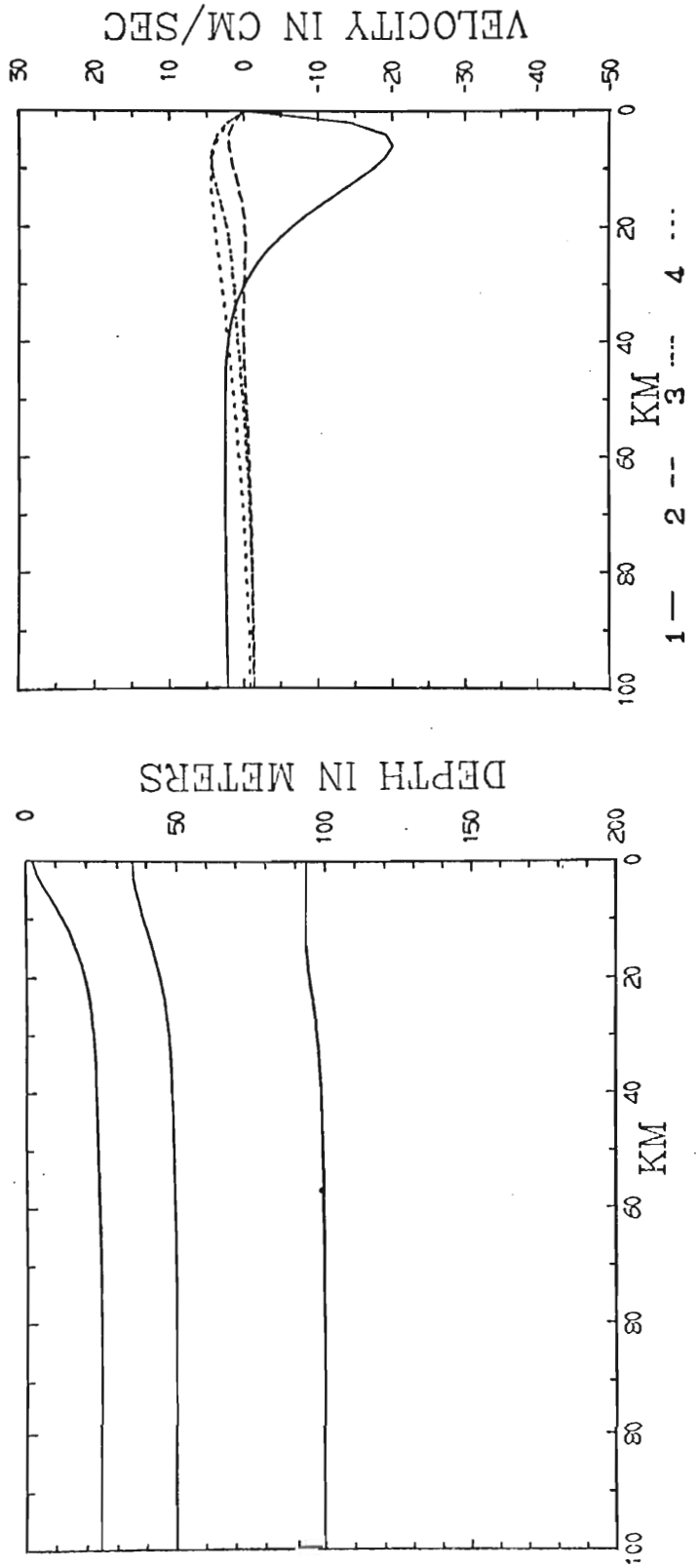

Fig. 8.-Height profiles (left) after 10.0 days model time. Downwarping can be noted in the lower interface at the coast. Velocity profiles (right) also shown after 10.0 days indicate a strong poleward undercurrent. Layer numbers are given in the legend above.

first interface reaches the sea surface 10.5 days after the winds are first applied. This time scale compares with 5.5 days for the case of no wind stress curl. Ekman suction due to the curl at the coast does increase the width of the upwelling zone.

The longshore velocity profiles in Fig. 8 show that the equatorward surface current has been reduced from -35 cm sec^{-1} after 5.5 days in the previous case to -20 cm sec^{-1} after 10 days for the present case. At the same time the poleward undercurrent is found to be much stronger with a positive velocity in the lower layer of 5 cm sec^{-1}. We also note that the flow is poleward in all three lower layers in contrast to the equatorward velocity found in the second layer for the case with no curl. The marked change in the longshore velocities can be explained using modified Sverdrup dynamics. Hurlburt and Thompson (1972) through a detailed scale analysis show that a Sverdrup balance does not hold in the upwelling zone. Nevertheless, the positive wind stress curl in the upwelling zone does contribute a positive Sverdrup component to the flow. This positive component would thus tend to increase the poleward flow in the lower layers and decrease the equatorward flow near the surface.

A notable feature of the height profiles found in this multi-layer model is the downwarping of the lower interface at the coast. This can be seen as a slight bulging shape to the third interface in Fig. 8. As we mentioned before the longshore flow is essentially in geostrophic balance with the baroclinic and barotropic east-west pressure gradients. The drop in the third interface is simply the geostrophic adjustment of

balance with the baroclinic and barotropic east-west pressure gradients.
The drop in the third interface is simply the geostrophic adjustment of the height field to the poleward undercurrent. The bulge or convex shape to the interface seems to be characteristic of the shape of isopycnals

observed at intermediate depths of upwelling regions. Yoshida (1967) gives some good examples of this structure of the isopycnals as observed off the California coast.

The drop of the interface at the coast reduces the effective depth of the actual upwelling motions. In this way the poleward undercurrent plays a significant role in determining the depth at which upward movement of water can occur.

The transverse circulation as given by the streamfunction in Figs. 9 and 10 shows basically the same pattern we found for the previous case with no curl. The main cyclonic circulation is still present although we note again the widening of the upwelling zone. Superimposed on the flow are the effects of several of the propagating internal waves. The amplitude of the waves are not as large for this case because the wind stress is less at the coast. A further discussion of the internal waves will be found in Section 5.

Using the same wind stress profile (Fig. 7) the model was run with a stratification $\Delta\sigma_t$ of 0.5, 2.0, 0.5. The model solutions are found in Fig. 12. Since the fluid is less stably stratified in the upper two layers than before, we expect higher vertical velocities and a more rapid rise of the first interface. This agrees with our solutions as the first interface surfaces after 7.8 days compared to 10.5 days for the more stably stratified case. This indicates the strong effect stratification exerts on the magnitude of the upwelling motions.

The longshore velocity field also shows a slight change due to the new stratification (compare Fig. 8 and Fig. 12). The equatorward surface

The longshore velocity field also shows a slight change due to the new stratification (compare Fig. 8 and Fig. 12). The equatorward surface jet is substantially reduced in the present case and, unlike the previous case, the jet extends into the second layer. If we use geostrophy in the

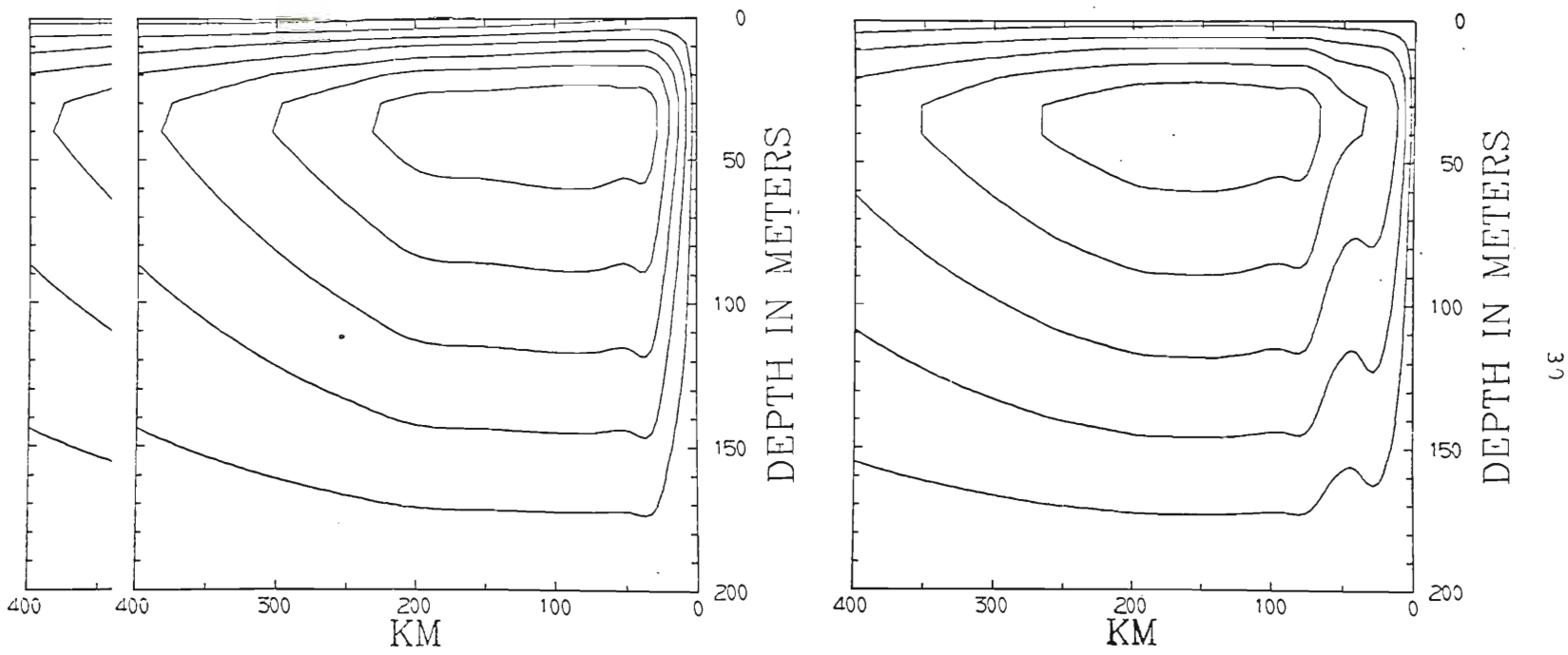

Fig. 9.-x-z streamfunction (left) after 1.0 days and (right) 2.0 days. Several internal waves can be seen superimposed on the flow.

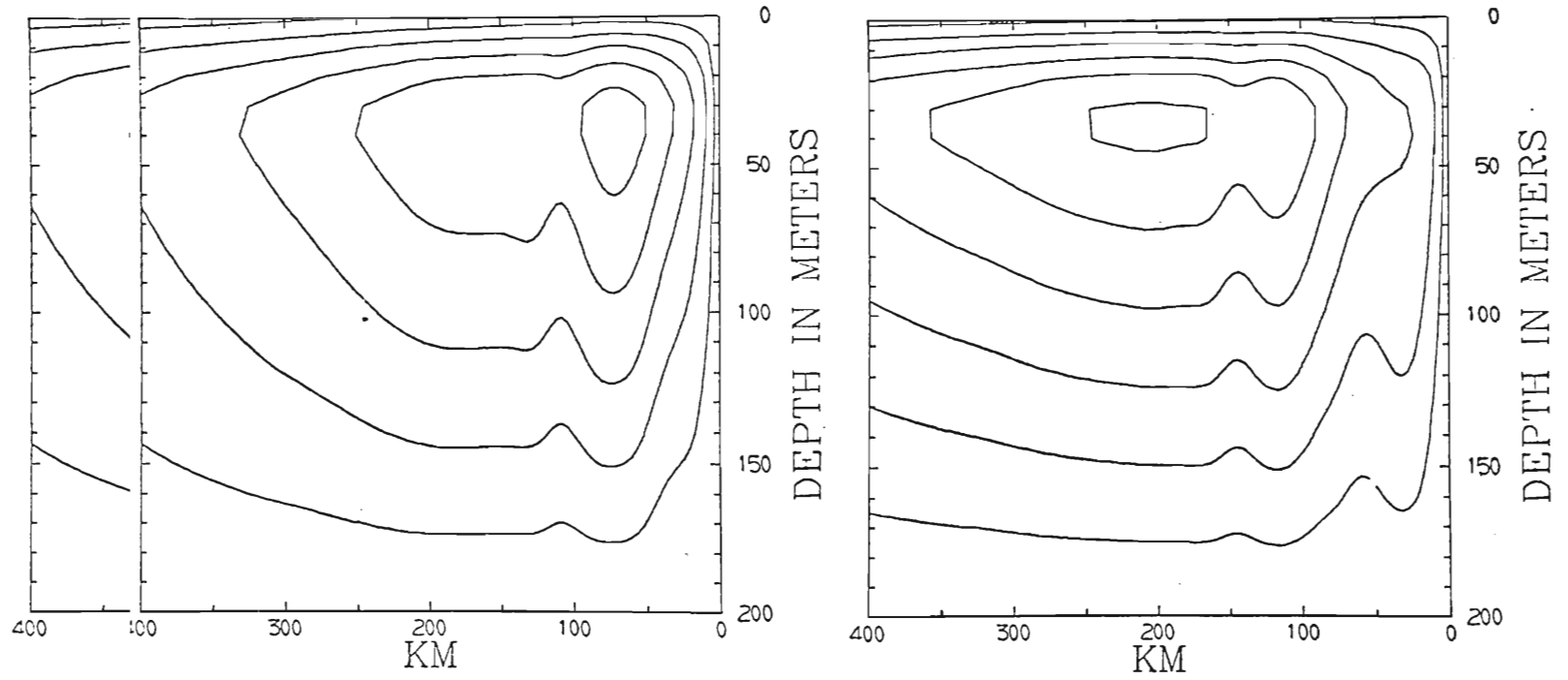

Fig. 10.-x-z streamfunction (left) after 3.0 days and (right) after 4.0 days.
The wavelength of the internal waves is observed to decrease as the waves move offshore.

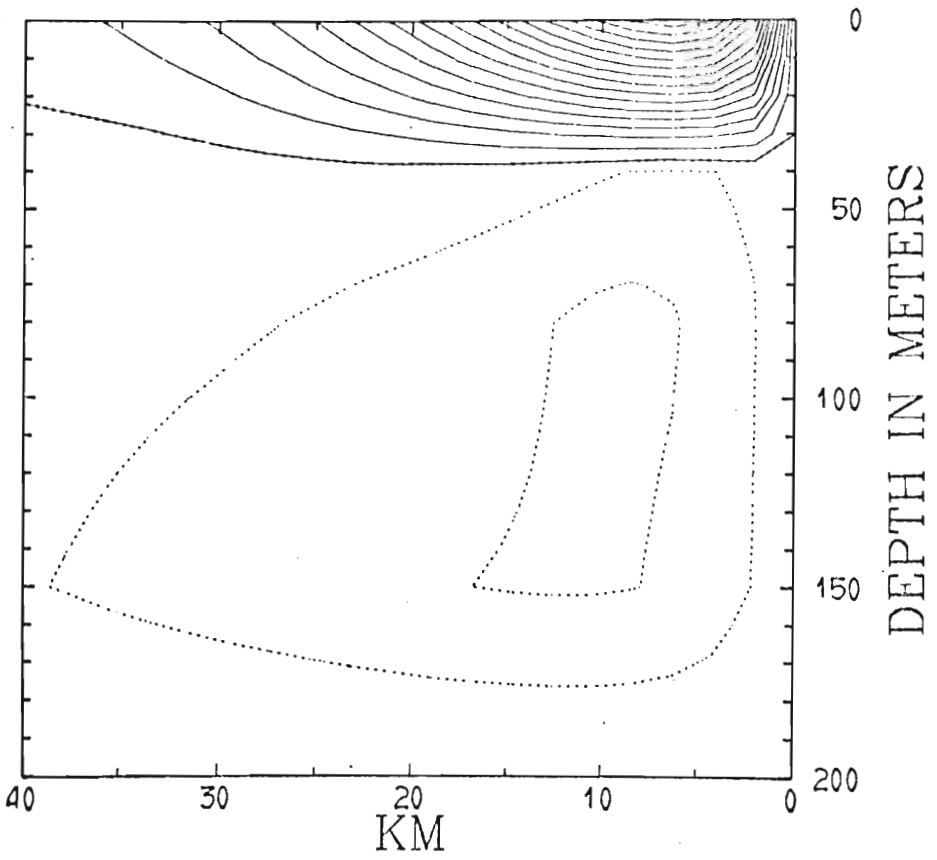

Fig. 11.-Longshore flow field contoured in the x-z plane after 10.0 days for the case with wind stress curl at the coast. Contour interval is 2 cm sec^{-1}. Values > 0 are shown by dashed lines.

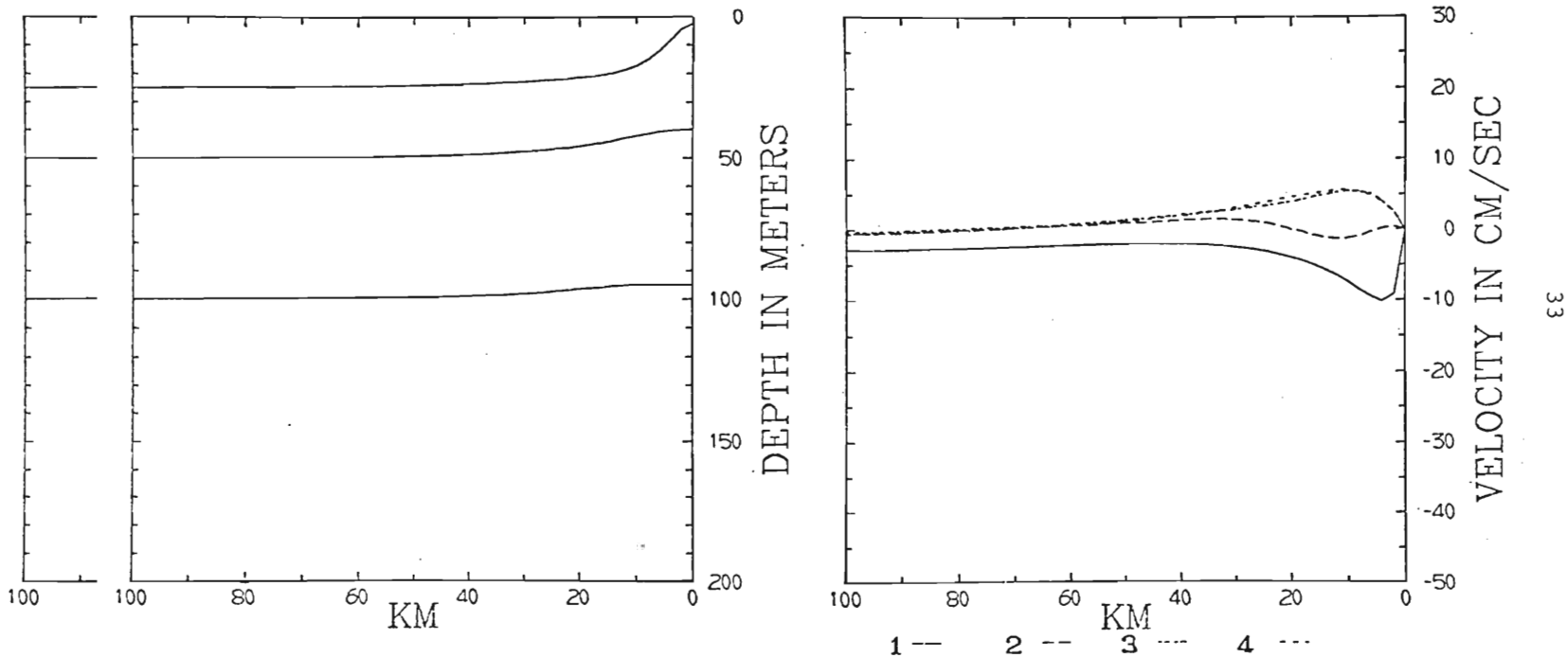

Fig. 12.-Height profiles (left) and velocity profiles (right) after 7.5 days model time. The stratification imposed is 0.5, 2.0, 0.5 and wind stress has curl at the coast.

longshore flow

$$f\,(v_1 - v_2) = g\,\varepsilon_{12}\,h_{1x} \qquad (25)$$

$$f\,(v_2 - v_3) = g\,\varepsilon_{23}\,(h_1 + h_2)_x\,, \qquad (26)$$

we can qualitatively explain the effect of stratification. Neglecting for the moment change in the slopes of the interfaces due to stratification, we find from (25) that, for a larger density contrast between the first and second layers, we expect a larger vertical shear in the longshore velocities. This concurs with our results for the $\Delta\sigma_t$ stratification of 2.0, 0.5, 0.5 (Fig. 8). Likewise, we would expect a smaller shear for the 0.5, 2.0, 0.5 case (Fig. 12). Comparing the slopes of the interfaces for the two cases, we find that h_{1x} is larger for the 2.0, 0.5, 0.5 case. This would further increase the shear between adjacent layers. Using (26) we note that a strong density contrast between layers 2 and 3 would coincide with a large difference between v_2 and v_3 as found in the second case. These simplified results are not complete since stratification has a direct effect on the width scale of the upwelling zone thus influencing the slope of the interfaces.

4.3 Oregon coast simulation

The last case we want to consider is a region with topography similar to that found off Newport, Oregon. This area is of interest because data collected by Oregon State University over many years can be used to compare with model results. Also a large scale field experiment is planned for the summer of 1972 to provide details of the upwelling

used to compare with model results. Also a large scale field experiment is planned for the summer of 1972 to provide details of the upwelling

structure and wind data. The geometry used in the model is shown in Fig. 13. Present model requirements dictate that the topography be

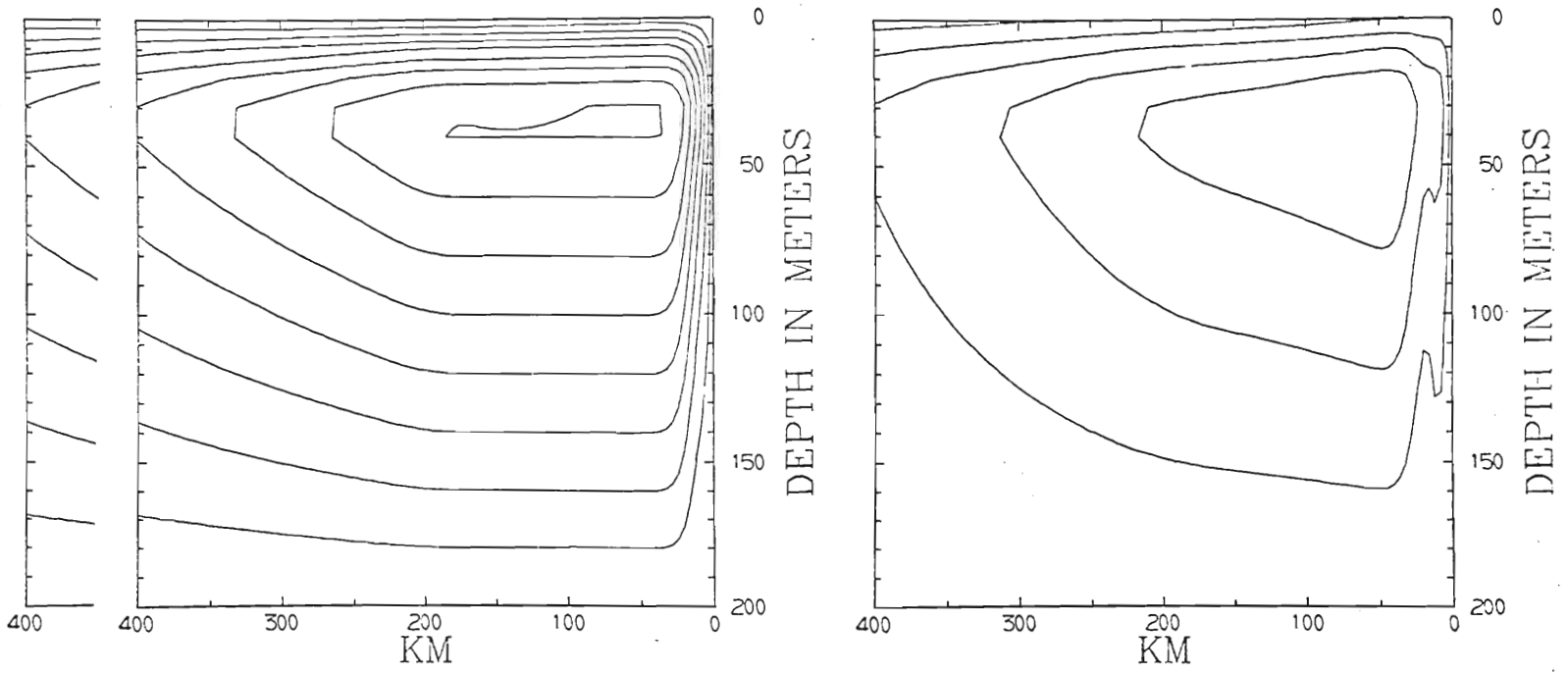

Fig. 3.-x-z streamfunction (left) after 0.4 days and (right) after 0.6 days model time. Distortion of the streamlines by an internal gravity wave can be observed near the coast. The main circulation is cyclonic.

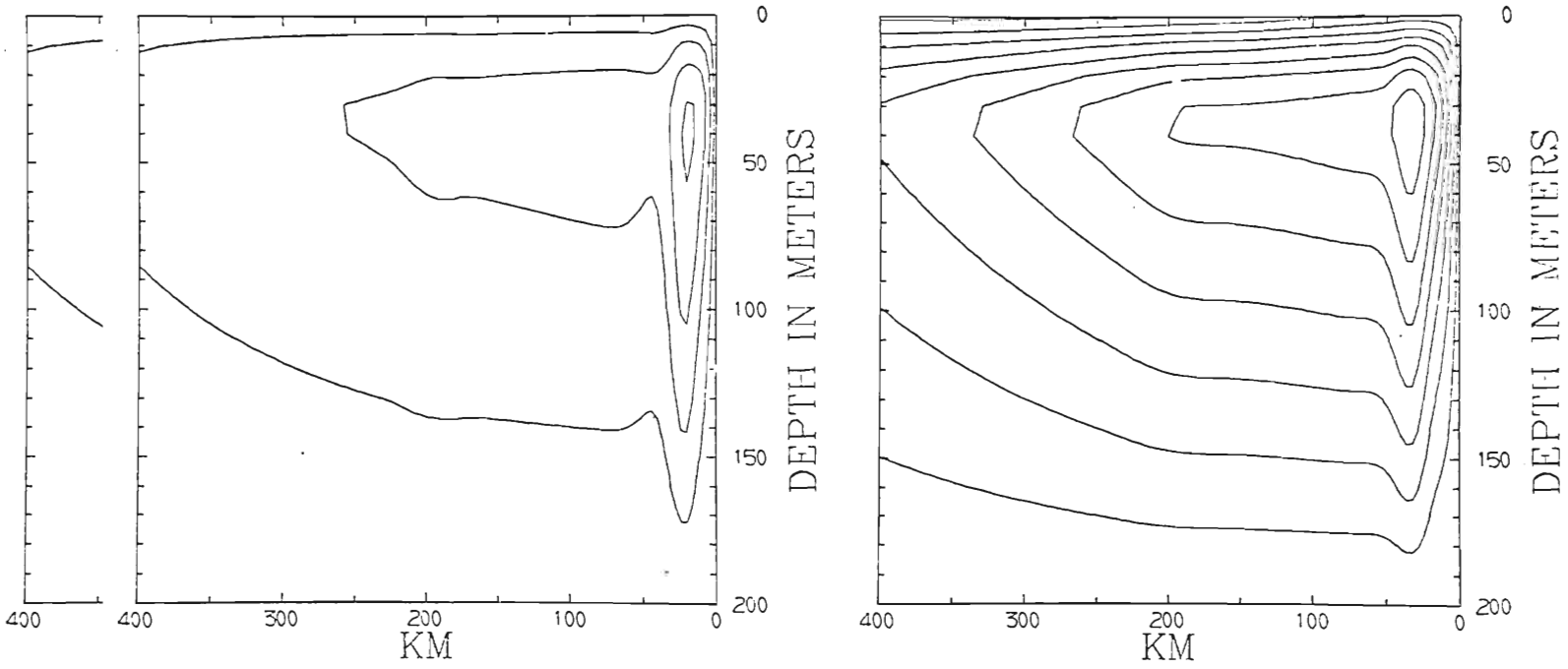

Fig. 4.-x-z streamfunction (left) after 0.8 days and (right) after 1.0 days model time. The propagating internal gravity wave is now a closed circulation. An inertial oscillation can be seen by an increase and decrease of streamlines.

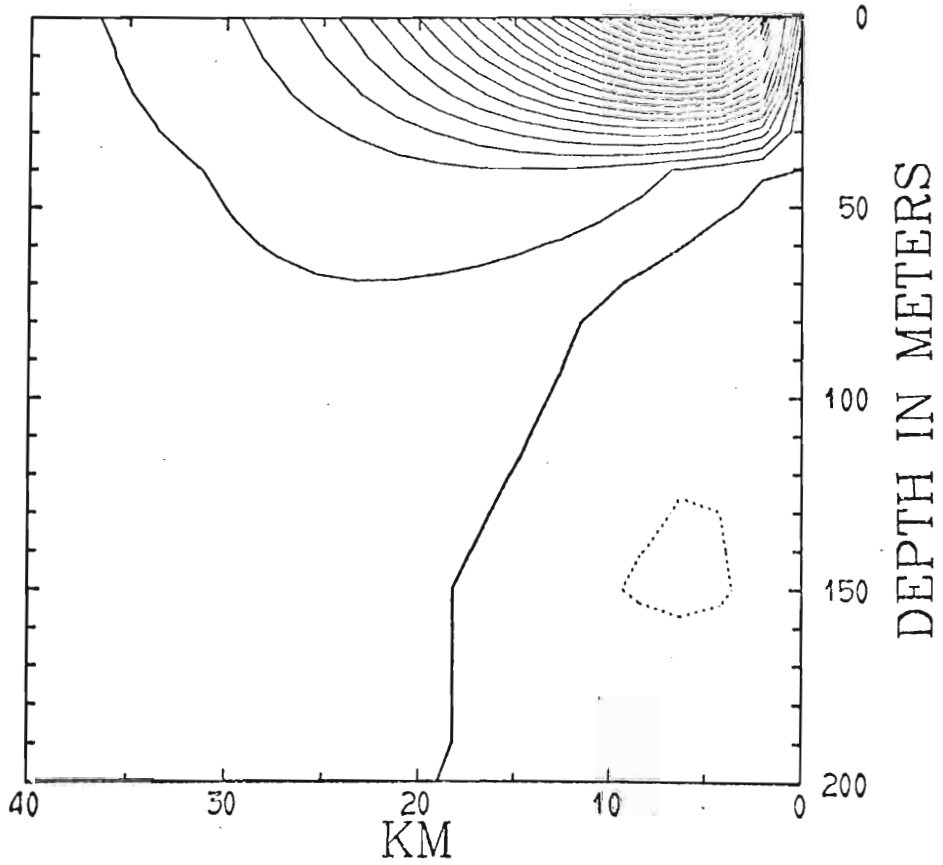

Fig. 5.-Longshore flow field contoured in the x-z plane after 5.5 days. A strong equatorward surface jet and poleward undercurrent can be observed. Contour interval is 2 cm sec^{-1}. Values > 0 are shown by dashed lines.

increasing depth. This width change and flattening of the interfaces near the coast will be related to the longshore velocity profiles subsequently.

Not shown in the accompanying diagrams is the offshore region 200 km to 700 km where the interfaces drop below their initial positions. This downwelling can be attributed to simple Ekman pumping induced by the negative curl in the wind stress. The unforced region beyond the downwelling region (700 km to 800 km) is characterized by essentially no displacement of the interfaces and near zero velocities.

Due to the impulsive starting of the wind stress the solutions exhibit a strong inertial character in early stages of spinup. In fact, the cross-stream flow as shown in the streamfunction diagrams of Figs. 3, 4 is clearly dominated by these oscillations. Recent oceanographic literature (e.g., Mooers, 1970) indicates strong inertial oscillation in nature. The inertial period for the model is 17.44 hours at $\approx 45°$ latitude. The sudden application of wind stress curl in the model also excites small amplitude Rossby waves of 1-2 cm sec^{-1} in the longshore velocity field.

Propagating internal gravity waves are shown as small closed circulations in Figs. 3, 4. The physical behavior and possible importance of these waves will be discussed later.

The strength of the upwelling produced depends to a large extent upon the imposed stratification. A large density contrast between the two upper layers inhibits vertical motion thus reducing the magnitude of
upon the imposed stratification. A large density contrast between the two upper layers inhibits vertical motion thus reducing the magnitude of
the upwelling. If the lower layers are more stably stratified than the upper layers then the strength of the upwelling is necessarily greater

in the upper levels. Hsueh and Kenny (1972) have shown a similar relationship (for a continuously stratified fluid).

We also notice the lowest interface is considerably flattened in comparison to the interfaces above. This can be attributed to the geostrophic adjustment of the layer to the poleward undercurrent. The importance of this downwarping will be discussed subsequently for a case which displays more dramatically this divergence of the interfaces.

As mentioned above, the width of the upwelling region at the coast increases with depth showing a very noticeable change between the first and second interfaces. This width difference results in a thinning of the second layer at approximately 12 km. Blumsack (1972) has shown, using boundary layer analysis techniques for a continuously stratified fluid, that the upwelling region below a surface Ekman layer spreads laterally with increasing depth.

The longshore flow is balanced geostrophically in all layers and is thus directly related to the height profiles mentioned above. The upper layer flow responds to sea-surface depression of 12 cm at the coast while the velocities in the lower layers are greatly modified by the baroclinic pressure gradients induced by the sloping interfaces. Hurlburt and Thompson (1972) show that the β-effect can produce a poleward undercurrent by inducing a north-south pressure gradient. The onshore flow in the lower layers is balanced by this longshore pressure gradient except near the coastal boundary. The kinematic boundary condition at the coast requires a breakdown in the onshore geostrophy. The resulting cross
near the coastal boundary. The kinematic boundary condition at the coast requires a breakdown in the onshore geostrophy. The resulting cross gradient flow give a northward component of motion allowing a poleward undercurrent to develop.

The tilt of the equatorward jet with depth mentioned earlier is an interesting feature of the four-layer model. To clarify our discussion of the tilt let us consider in place of the beta model an f-plane model in which no poleward undercurrent can exist. The solutions for the f-plane case may be found in Fig. 6. The stratification imposed is $\Delta\sigma_t$ of 0.5, 0.2, 0.5, with a constant wind stress near the coast of -1.0 dynes cm^{-2}. The dominant feature in the longshore profiles is the strong equatorward jet in the upper layer extending into the second layer with a slight tilt offshore. If we look at the accompanying height profiles we again see the sharp increase in the width of the upwelling zone between the first and second layers.

O'Brien and Hurlburt (1972) have explained the presence of the longshore jet in the upper layer using conservation of potential vorticity. Consider the following equations where we have neglected horizontal friction and interfacial stresses

$$\frac{\partial v_1}{\partial t} + u_1 \frac{\partial v_1}{\partial x} + f u_1 = \tau^{sy}/\rho H_1 \qquad (12)$$

$$\frac{\partial v_j}{\partial t} + u_j \frac{\partial v_j}{\partial x} + f u_j = 0 \qquad j = 2(1)4 \qquad (13)$$

$$\frac{\partial h_j}{\partial t} + \frac{\partial}{\partial x}(h_j u_j) = 0 \qquad j = 1(1)4 \qquad (14)$$

We may form the following potential vorticity equation for each layer

layer $\left(\frac{\partial v}{\right.}$ $\left.\right)$

$$\frac{d}{dt}\left(\frac{\frac{\partial v_j}{\partial x} + f}{h_j}\right) = 0 \qquad j = 1(1)4 \qquad (15)$$

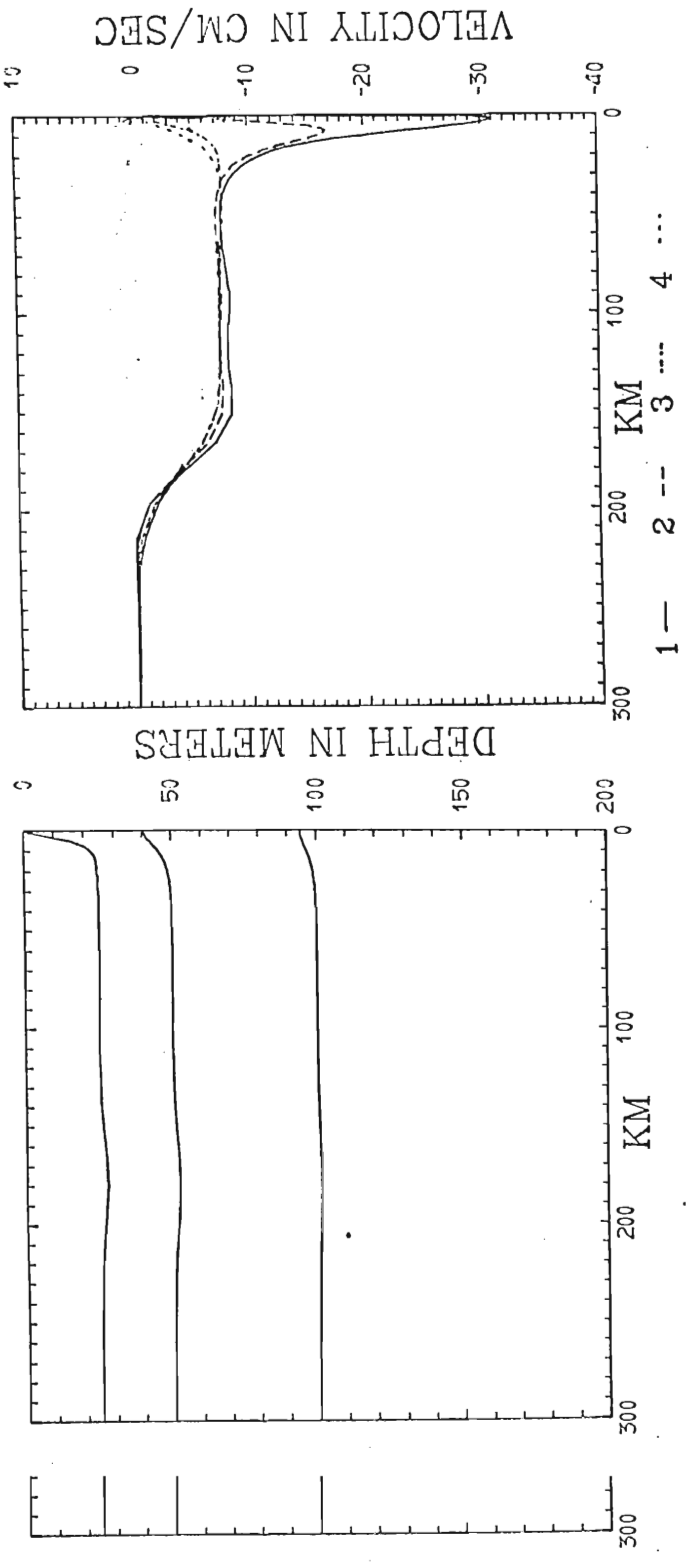

Fig. 6.—Height profiles (left) after 1.8 model time. Velocity profiles (right) also after 1.8 days. Both diagrams are for f-plane model with constant wind stress near the coast of 1 dyne cm-2 and stratification of 0.5, 2.0, 0.5. Layer numbers are given in legend above.

After integrating once along a trajectory and using the initial conditions we obtain

$$\frac{\partial v_j}{\partial x} = f\left[\frac{h_j - h_{j0}}{h_{j0}}\right] \qquad (16)$$

with h_{j0} the initial layer thickness of a layer j at t = 0.

Upwelling at the coast implies $h_{10} > h_1$ so v_1 must have a relative minimum at the coast. Horizontal friction which brings the longshore flow to zero at the boundary will displace the minimum away from the shore. Thus a longshore equatorward jet is predicted in the upper layer with the strongest flow slightly offshore. For a two-layer model this jet is necessarily confined to the upper layer.

In the second layer we find in the upwelling region that $h_{20} \leq h_2$ everywhere except in the vicinity of 12 km where the second layer is thinned in response to the width difference of the upwelling zone between the two layers. This thinning of the layer implies a change of sign of the vorticity and an inflection point in the velocity field. The point of inflection is a relative minimum giving an equatorward jet in the second layer near the region of maximum thinning. Thus conservation of vorticity predicts an equatorward jet extending at least through the second layer with the jet axis tilted offshore.

Stratification plays an important role in the structure of the longshore coastal currents since certain density profiles tend to enhance the features responsible for the formation of the jet. A vertical density profile in which the biggest contrast occurs between the first and second the features responsible for the formation of the jet. A vertical density profile in which the biggest contrast occurs between the first and second layers inhibits the formation of a minimum in the second layer by reducing the thinning effect mentioned above. Stratification more conducive to

upwelling increases the thinning and strengthens the jet in the second layer. The increased thinning in this case could be attributed simply to the greater upward movement of the second interface. However, boundary layer analysis may show stratification to be important in determining the width scale of the upwelling zone. An increase in scale width would also contribute to the thinning of the second layer.

The same type of argument is valid for the β-plane model thus explaining the tilt in the jet axis as seen in Fig. 3. The formation of the poleward undercurrent in the model complicates the argument in the lower layers. However, we can develop certain relations which predict fairly well the structure of the longshore velocity field in the β-plane model.

Let us return to the β-plane solutions discussed earlier and shown in Fig. 3. An interesting feature of the beta model is that the vertical integral of the longshore transport is approximately zero near the shore where the wind stress is constant. This can be verified directly from the solutions or derived using a scale analysis of the model equations (see Hurlburt and Thompson, 1972). We want to use this fact and geostrophy in the longshore flow to derive relations governing the velocity profile near the coast.

We will simplify our analysis by considering a three-layer system in which the net longshore transport is zero so that

$$v_1 h_1 + v_2 h_2 + v_3 h_3 = 0 . \qquad (17)$$

The procedure we will follow can be carried out for the four-layer model.

The procedure we will follow can be carried out for the four-layer model.

However, the final results and their discussion can more easily be presented using only three layers. Assuming geostrophy in (4) we obtain

$$f\,(v_1 - v_2) = g\,\varepsilon_{12}\,h_{1x} \tag{16}$$

and

$$f\,(v_2 - v_3) = -\,g\,\varepsilon_{12}\,h_{1x} + g\,\varepsilon_{13}\,h_{1x} + g\,\varepsilon_{23}\,h_{2x} \tag{19}$$

However,

$$\varepsilon_{13} = \varepsilon_{12} + \varepsilon_{23}$$

therefore

$$f\,(v_2 - v_3) = g\,\varepsilon_{23}\,(h_{1x} + h_{2x})\ . \tag{20}$$

We can solve (14), (15) and (17) for the three longshore velocities to obtain

$$v_1 = \frac{g\,\varepsilon_{12}(h_2 + h_3)\,h_{1x}}{f\,H_T} + \frac{g\,\varepsilon_{23}\,h_3(h_1 + h_2)_x}{f\,H_T} \tag{21}$$

$$v_2 = \frac{-\,g\,\varepsilon_{12}\,h_1\,h_{1x}}{f\,H_T} + \frac{g\,\varepsilon_{23}\,h_3(h_1 + h_2)_x}{f\,H_T} \tag{22}$$

$$v_3 = \frac{-\,g\,\varepsilon_{12}\,h_1\,h_{1x}}{f\,H_T} - \frac{g\,\varepsilon_{23}(h_1 + h_2)(h_1 + h_2)_x}{f\,H_T} \tag{23}$$

where

$$H_T = h_1 + h_2 + h_3 \tag{24}$$

These relations can be used to explain qualitatively the velocity regime we would expect in the three-layer system. If upwelling is present then $h_{1x} < 0$ and $(h_1 + h_2)_x < 0$ except when downwarping of the second interface occurs with a strong poleward countercurrent. Also from our solutions we see generally that in absolute magnitude $\left|h_{1x}\right| \geq \left|(h_1 + h_2)_x\right|$. With this in mind we note in (21) that v_1 should be negative (e.g., equatorward flow).

see generally that in absolute magnitude $\left|h_{1x}\right| \geq \left|(h_1 + h_2)_x\right|$. With this in mind we note in (21) that v_1 should be negative (e.g., equatorward flow).

Eq. (22) predicts a poleward flow in the bottom layer since both terms would make a positive contribution to the longshore velocity in the layer.

$$q = (u_j^2 + v_j^2)^{1/2} \quad ; \quad \bar{q}_j = (q_{j+1} + q_j)/2$$

$$\tau_j^{Tx} = \rho\, c_I\, \bar{q}_j^{T}\, (u_{j-1} - u_j) \quad , \qquad j \neq 1$$

$$\tau_j^{Bx} = \rho\, c_I\, \bar{q}_j^{B}\, (u_j - u_{j+1}) \quad , \qquad j \neq n$$

$$\tau_j^{Ty} = \rho\, c_I\, \bar{q}_j^{T}\, (v_{j-1} - v_j) \quad , \qquad j \neq 1$$

$$\tau_j^{By} = \rho\, c_I\, \bar{q}_j\, (v_j - v_{j+1}) \quad , \qquad j \neq n$$

$$\tau_j^{Bx} = \rho\, c_B\, q_j\, u_j \quad ; \quad \tau_j^{By} = \rho\, c_B\, q_j\, v_j \qquad j = n$$

for which

ρ - density for layer

c_I - interfacial stress constant

c_B - bottom stress constant.

The subscript j refers to the layer number with numbers increasing downward from the surface layer. Each layer is assumed to be homogeneous and the horizontal components u_j, v_j are assumed independent of depth within the layer.

The symbols τ_j^{T} and τ_j^{B} are the stresses at the top and bottom of each layer and are formulated such that stresses are continuous across the interfaces. Note that for $j = 1$, τ_j^{T} becomes the wind stress at the sea surface and may be specified as a function of x and t. Bottom topography is included through D(x) which represents the height of the bottom above a deep reference level.

The model parameters ρ, g, f, A, c_I, C_B, β are specified initially and may be found in Table 1. We have chosen interfacial stress constants

and may be found in Table 1. We have chosen interfacial stress constants to be identical for all layers. Thompson and O'Brien (1972) have estimated that $c_I = 10^{-5}$ and $c_B = 10^{-3}$ in cgs units are realistic parameter values for upwelling on a continental shelf.

Table 1.-List of symbols and model constants

$f = 10^{-4}\ \text{sec}^{-1}$	Coriolis parameter
$g = 980\ \text{cm sec}^{-1}$	acceleration of gravity
$\rho_1 = 1.0\ \text{g cm}^{-3}$	density of the top layer
$A = 10^{6}\ \text{cm}^{2}\ \text{sec}^{-1}$	coefficient of horizontal friction
$c_I = 10^{-5}$	internal stress coefficient in cgs units
$c_B = 10^{-3}$	bottom stress coefficient in cgs units
$\beta = 2\times10^{-13}\ \text{cm}^{-1}\ \text{sec}^{-1}$	variation of Coriolis parameter
	$\beta = \frac{df}{dy} = \text{constant}$
u	x - directed component of motion
v	y - directed component of motion
w	z - directed component of motion
τ^{Sy}	y - directed wind stress
τ^{Sx}	x - directed wind stress
u_E	Ekman transport
h	layer thickness

The time-dependent equations (1 to 3) represent a closed system with dependent variables u_j, v_j, and h_j. Boundary conditions are u_j, $v_j = 0$ at the coast and in the far field. Layer thicknesses at the coast are calculated using a one-sided finite difference in the continuity equation. Initially the stratified fluid is at rest.

The curl of the momentum equations yields an equation for the vertical component of relative vorticity for each layer. If we assume that the velocity field is independent of y and that non-linear terms that include longshore variations in y may be neglected in the vorticity and continuity equations, the equations for a multi-layer model ocean may be written

$$\frac{\partial u_j}{\partial t} + u_j \frac{\partial u_j}{\partial x} = f v_j - g \sum_{i=1}^{n} \frac{\partial h_i}{\partial x} - g \frac{\partial D}{\partial x}$$

$$+ g \sum_{i=1}^{j-1} \varepsilon_{ij} \frac{\partial h_i}{\partial x} + \left(\tau_j^{Tx} - \tau_j^{Bx}\right)/\rho h_j + A \frac{\partial^2 u}{\partial x^2} \qquad (4)$$

$$\frac{\partial}{\partial t} \frac{\partial v_j}{\partial x} + \frac{\partial}{\partial x}\left(u_j \frac{\partial v_j}{\partial x}\right) + f \frac{\partial u_j}{\partial x} + \beta v_j$$

$$= \frac{\partial}{\partial x}\left(\left(\tau_j^{Ty} - \tau_j^{By}\right)/\rho h_j\right) + A \frac{\partial^3 v_j}{\partial x^3} \qquad (5)$$

$$\frac{\partial h_j}{\partial t} + \frac{\partial}{\partial x}\left(u_j h_j\right) = 0 \qquad (6)$$

where

$$\beta = \frac{df}{dy} = \text{constant.}$$

$$\beta = \frac{df}{dy} = \text{constant.}$$

An additional boundary condition is required by (5). Hurlburt and Thompson (1972) have demonstrated that for an inert, unforced far field it is consistent to assume that the longshore pressure gradient vanishes

at some distance remote from the coast. This is equivalent to assuming

$$\frac{\partial^2 v_j}{\partial x^2} = 0 \qquad (7)$$

at the computational boundary off-shore.

We will solve (4) - (6) for a four-layer system. The twelve equations are solved numerically using the economically efficient semi-implicit scheme developed by Kwizak and Robert (1971) and O'Brien and Hurlburt (1972). The implicit treatment of both the external and internal gravity waves permits a substantial increase in computational speed.

3. MODEL DISPLAY

The numerical solutions to (4) - (6) yield profiles of u_j, v_j, and h_j as a function of x and t. Since the velocity is independent of y, it should be possible to define a streamfunction in the x-z plane. However, u_j represents an average over the layer and the vertical velocity w_j is defined only at the interface between layers and at the sea surface. In order to display the solutions in a pictorial form which is more easily understood, we elect to treat the velocity field as continuous in z. The u_j and v_j are regarded as estimates of the velocity components at the center of each layer. Using linear interpolation between layers and linear extrapolation above mid-depth of the surface layer, it is possible to generate a continuous profile of u. Similarly, we can interpolate linearly between the 5 w's to obtain a continuous profile for w. If we assume that this modified u, w field satisfies

$$\frac{\partial u}{\partial x} + \frac{\partial w}{\partial z} = 0 \qquad (8)$$

we may define a streamfunction ψ where

$$\frac{\partial^2 \psi}{\partial x^2} + \frac{\partial^2 \psi}{\partial z^2} = \frac{\partial u}{\partial z} - \frac{\partial w}{\partial x} = \eta$$

and η is the y component of the vorticity vector $\vec{\nabla} \times \vec{v}$.

The vertical velocity at any interface, j, is

$$w_j(x,t) = \sum_{i=j}^{n} \frac{d}{dt} h_i + \frac{d}{dt} D \qquad (9)$$

$$\sum_{i=j}^{n}$$

where w_1 is vertical movement of the sea surface and D is the topography height. The vertical velocity at the bottom w_B is

$$w_B = \frac{dD}{dt} \; . \qquad (10)$$

The streamfunction, ψ, is zero at the coast, along the bottom and at the computational boundary. Along the surface ψ does not vanish. We calculate ψ at the free surface from

$$\frac{\partial^2 \psi}{\partial x^2} = - \frac{\partial w}{\partial x} \qquad (11)$$

with boundary conditions $\psi = 0$ at the coast and in the far field. A finite difference analogue of this equation is solved using the tri-diagonal variant of Gaussian elimination. The interior solution for ψ is found using a standard over-relaxation procedure. Contours of ψ in the x-z plane contain all the information of the u_j and h_j profiles. This procedure should be regarded only as a convenient method to display the solutions for the four-layer model.

We may also interpolate v_j to obtain a continuous profile of v. Contours of the longshore velocity are a convenient way to display the model solutions. No new information content has been introduced by the interpolation. Between layers, the gradients are linear. One may easily construct the computed v_j from the contoured x-z distributions of the longshore velocity.

4. RESULTS

Many model cases have been run exploring various vertical density profiles, layer thicknesses, wind stress and bottom topography. We have singled out three cases with which to explain the essential physics and results of the model. We will mention additional cases where applicable to better focus on a particular result.

4.1 Flat shelf case

We shall first consider the circulation on a wide flat oceanic shelf. The fluid depth is taken to be 200 meters with layer thicknesses $h_1 = h_2 = 25$ m, $h_3 = 50$ m, $h_4 = 100$ m (see Fig. 1). The east-west model width is 800 km; however, we shall generally only be concerned with solutions near the coast (< 200 km). The wind stress imposed for this case is given in Fig. 1. Three distinct regions may be identified; a constant wind stress region inward of 200 km, a region with wind stress curl 200-700 km, and an unforced outer region 700 km to 800 km.

Model stratification will be expressed in terms of density contrasts across the interfaces in σ_t units. The vertical density profile for this case is constructed so that there is a density difference of 2.0×10^{-3} g cm^{-3} between the first and second layers and differences of 5×10^{-3} g cm^{-3} between the remaining layers. The corresponding $\Delta\sigma_t$ units are 2.0, 0.5, and 0.5.

All model cases were run with the fluid initially at rest at t = 0. The wind stress was applied impulsively and maintained until the interface between the first and second layers reached the sea surface. (Hereafter, we shall refer to this uppermost internal interface as the first interface and so forth.)

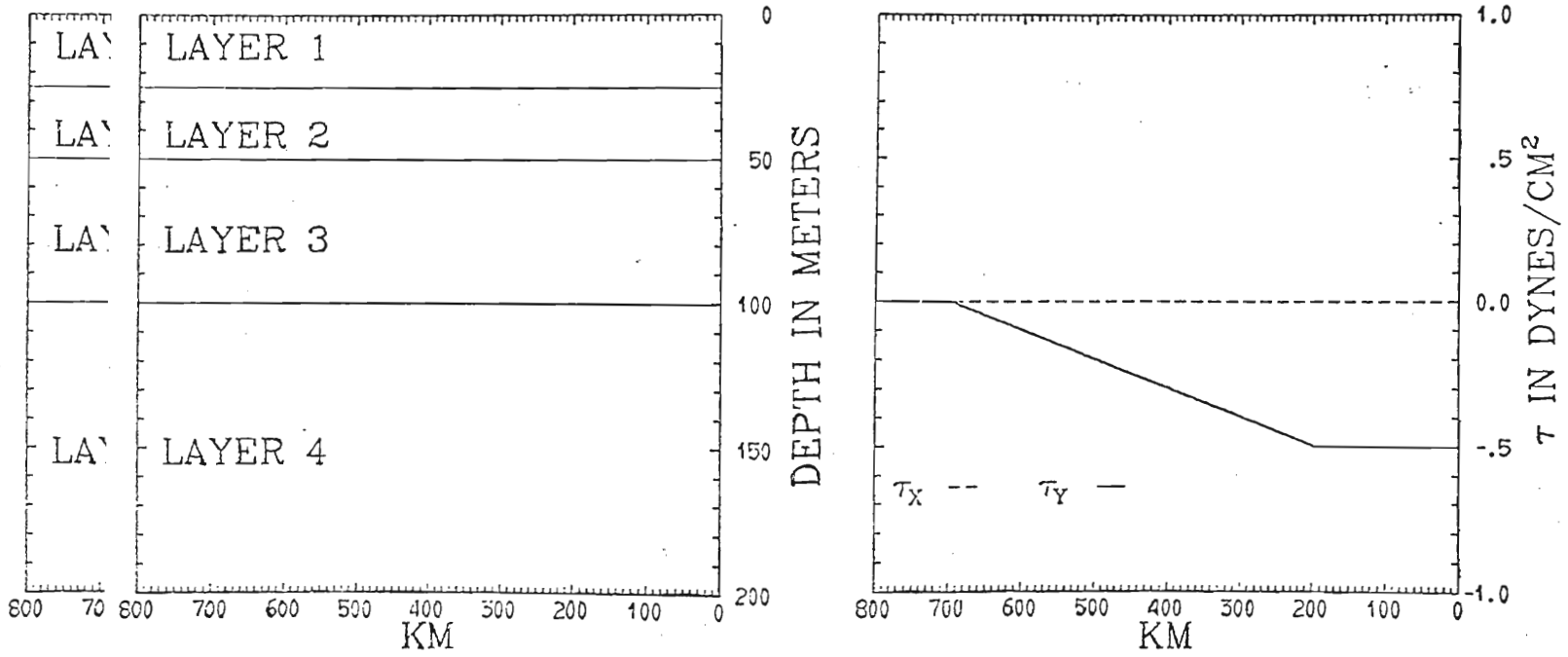

Fig. 1.-Initial conditions (left) u = v = 0, $h_1 = h_2 = 25$ m, $h_3 = 50$ m, $h_4 = 100$ m. Wind stress components (right) as a function of distance offshore; τ_{sy} is - 0.5 dynes cm^{-2} at the coast; τ_{sx} is zero everywhere.

The solutions after 5.5 days for this first model case are shown in Figs. 2-5. The diagrams show velocity and height profiles shoreward of 100 km and streamfunction for half the model region.

Offshore transport as predicted by classical Ekman dynamics is confined to the upper layer. Onshore flow required by continuity is essentially evenly distributed throughout the lower three layers. This is the first important result of the multi-layer model.

Longshore velocity profiles (Fig. 2, right) show a fairly strong equatorward jet in the upper layer of -35 cm sec^{-1} at 8 km. Horizontal friction in the model requires the velocity to vanish at the coast. In the absence of horizontal friction the jet minimum will occur at x = 0. The longshore velocity in the second layer is weaker with a minimum of -5 cm sec^{-1} at approximately 12 km. This offshore tilt of the jet will be discussed subsequently. The lower two layers exhibit a poleward flowing countercurrent as observed by Mooers, Collins, and Smith (1972), in upwelling regions with maximum velocity in the bottom layer.

The accompanying height profiles (Fig. 2, left) show the position of the interfaces at 5.5 days. At the coast all three interfaces have moved upward from their initial positions in response to the one-sided divergence at the coast. However, the displacement is less with increasing depth; e.g., the third interface has risen only about one-third the distance of the first interface. This corresponds to a mean vertical velocity in the upper layer of $w \approx 5\times10^{-3}$ cm sec^{-1} and $w \approx 1.5\times10^{-3}$ cm sec^{-1} in the bottom layer.

velocity in the upper layer of $w \approx 5\times10^{-3}$ cm sec^{-1} and $w \approx 1.5\times10^{-3}$ cm sec^{-1} in the bottom layer.

Although vertical velocities are smaller near the bottom a noticeable increase in the scale width of the upwelling region is observed with

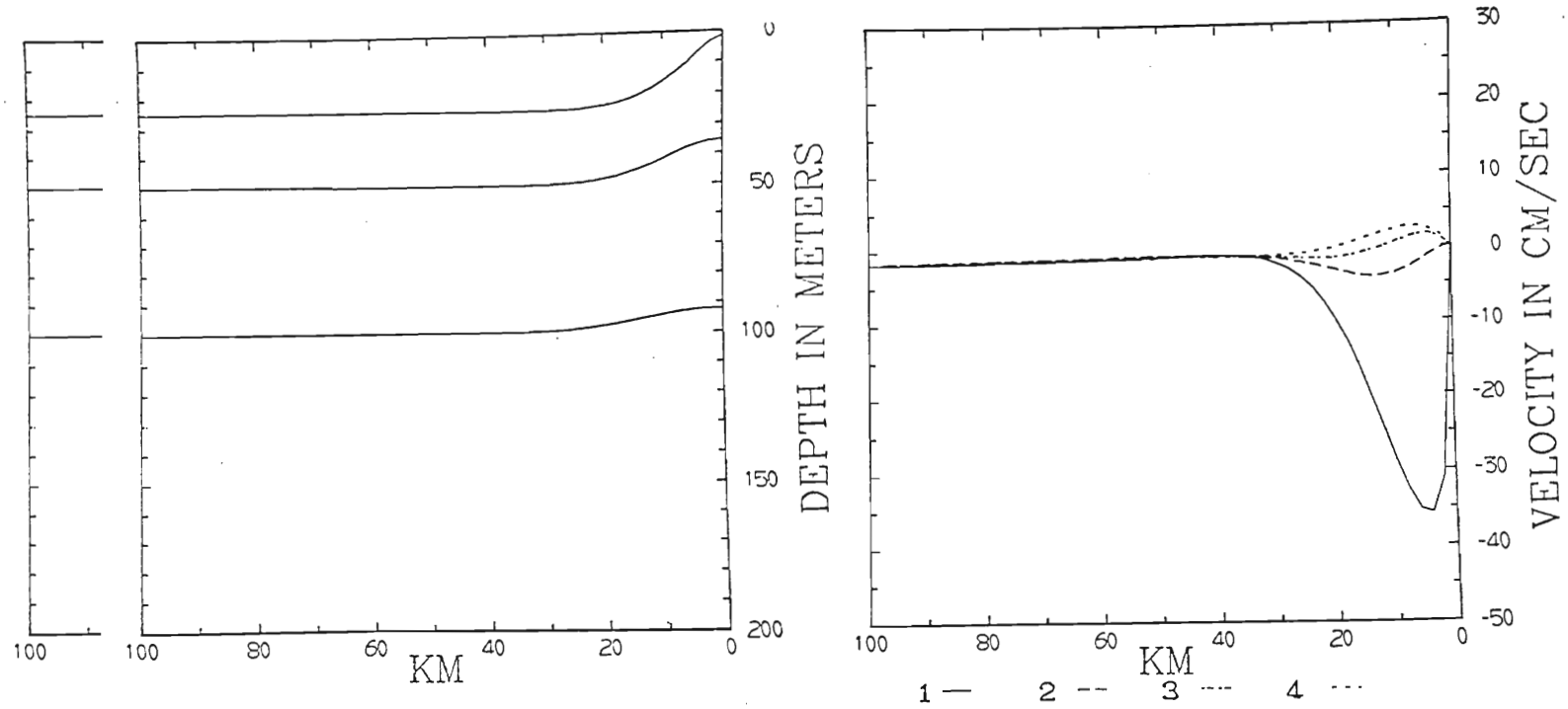

Fig. 2.-Height profiles (left) after 5.5 model days. Upwelling is indicated at the coast by the upturning of the interfaces. Longshore velocity profiles (right) are shown also after 5.5 days. Both diagrams are for the β-model with imposed stratification $\Delta\sigma_t$ of 2.0, 0.5, 0.5. Layer numbers are given in legend above.

ABSTRACT

Wind-driven coastal upwelling in a rotating, stratified ocean is simulated using a four layer numerical model. All longshore variations in the velocity field are neglected. The beta effect and longshore pressure gradients are included. The vertical structure of the nearshore upwelling zone is emphasized and offshore Ekman drift is found to be confined to the surface layer while onshore flow is evenly distributed in the lower three layers. An investigation of the baroclinic coastal current reveals an equatorward surface jet and a weaker poleward undercurrent in the β-plane solutions. The vertical structure of these coastal currents is dependent upon the stratification imposed. A pronounced tilt away from the coast with depth is observed in the coastal jet. A noticeable down-warping of the lower interface is detected after the poleward undercurrent is established. Streamfunction representation of the transverse circulation indicates propagating internal waves due to the impulsively imposed wind stress are trapped within the first 200 km of the coast.

ACKNOWLEDGMENTS

This thesis resulted from the implementation of a four-layer model of coastal upwelling based upon a multi-layer model formulated by Professor James J. O'Brien and Harley E. Hurlburt, both of Florida State University. The author has contributed to the specific design of the four-layer model and the interpretation of the numerical solutions.

This research has been supported for the past eighteen months by the Office of Naval Research and the National Science Foundation under Grant No. GA-29734. Some research was carried on at the National Center for Atmospheric Research, Boulder, Colorado. NCAR is supported by the National Science Foundation.

The Computer Facility at NCAR provided some CDC 7600 and 6600 time while the Florida State University Computing Center provided CDC 6400 time.

The deepest appreciation is extended to Professor O'Brien for initiating and guiding this research, and to Harley Hurlburt and Dana Thompson for their invaluable assistance. Appreciation is also extended to Dr. Raymond Staley, Dr. David Loper, Dr. Ya Hsueh, and John Kindle for their helpful suggestions.

A special appreciation to my wife Martha, for her patient
Kindle for their helpful suggestions.

A special appreciation to my wife Martha, for her patient
understanding throughout the research.

TABLE OF CONTENTS

LIST OF ILLUSTRATIONS

LIST OF ILLUSTRATIONS - Continued

1. INTRODUCTION

Coastal upwelling is a well observed phenomenon along coastlines where an equatorward wind exists parallel to a coast. Under these conditions, offshore transport as predicted by Ekman (1905), will develop in response to the Coriolis acceleration. To satisfy continuity requirements at the boundary subsurface water must be brought to the surface in a region near the coast. This local phenomenon has a tremendous impact upon the marine biological production by providing a mechanism in which nutrient-rich subsurface waters can be brought to a level where sunlight is available. The combination of sunlight and nutrients is conducive to photosynthesis in small one-cell plants-phytoplankton. These plants provide a base for a complex food chain which can ultimately support large fish populations. Thus, upwelling areas are important fish producing regions for the world fishing industry.

The cold upwelled water present at the suface also has a dramatic effect on the climate by cooling the air temperature and increasing the relative humidity. The humid Peruvian coastal deserts are prime examples of climate modification induced by upwelling processes. Smith (1968) provides an excellent review article on the basic dynamics and effects of upwelling.

The present investigation is concerned with the vertical structure of the upwelling circulation. Since the temperature and nutritive con-

The present investigation is concerned with the vertical structure of the upwelling circulation. Since the temperature and nutritive con-tent of a water mass is essentially dependent upon its depth of origin,

a detailed description of the return flow is needed to understand the effect upwelling will exert on the environment. We will be specifically concerned with coastal upwelling induced by a steady wind blowing parallel to a north-south coastline. A multi-layer model patterned after the models of O'Brien and Hurlburt (1972), and Hurlburt and Thompson (1972) is utilized in the study of a simplified four-layer ocean. Simplifications include a hydrostatic fluid, constant density within the layers, and north-south symmetry in the velocity field. The wind stress forcing applied at the model surface is steady but not uniform across the model region and is applied impulsively at t = o. Longshore pressure gradients, the β-effect, and transfer of momentum between layers are included. Both internal and external gravity waves are present in the solutions and are excited by the impulsive start of the wind stress.

Dependent variables include layer thicknesses and horizontal velocity components within the layers. Vertical velocity can be calculated diagnostically from the above variables.

The model equations are integrated numerically for a wide, flat oceanic shelf of 200 m depth and a simulated Oregon coast case. Several different density profiles are used to investigate the effect of stratification on the strength of the upwelling and vertical structure of the longshore flow. A downwarping of isopycnals which reduces the effective depth of upwelling motions is found to be associated with a poleward flowing undercurrent.

A previous simulation of coastal upwelling by O'Brien and Hurlburt (1972) produced a realistic width to the upwelling region at the coast and an equatorward surface jet which is observed in upwelling regions.

Hurlburt and Thompson (1972) using a formulation which allowed inclusion of the β-effect and longshore pressure gradient were able to produce a more realistic longshore velocity profile that included a poleward undercurrents. Both of the above models contained only two layers and thus little detail of the vertical structure was available. The present investigation is an outgrowth of the above-mentioned work.

Analytical steady state models such as those of Yoshida (1967) and Hsueh and Kenny (1972) include thermohaline mixing which has been neglected in our formulation.

Observational data which are essential for model comparison, are unfortunately not complete. However, some of the best data available taken off the Oregon coast indicate a scale width for the upwelling zone of 15-25 km and vertical velocity of 30-60 meters per month. Geostrophic currents for a two-week average (Mooers, Collins, and Smith, 1972) reveal a surface equatorward current of - 20 cm/s and a poleward undercurrent of 10 cm/s at approximately 150 m depth. Other data along with further discussion of theoretical work will be cited in the course of the text where needed for comparison or documentation.

2. MODEL FORMULATION

The brief discussion of the model equations and geometry used in this investigation follows O'Brien and Hurlburt (1972) and Hurlburt and Thompson (1972). A vertical vorticity equation permits the inclusion of the β-effect and longshore pressure gradient. For a detailed derivation of the equations of motion the reader should consult this earlier work.

Consider the governing equations for a multi-layer ocean using a right-handed Cartesian coordinate system with z increasing upwards and x increasing to the east. The origin is chosen at the coast such that distances measured offshore are negative. In general form the vertically integrated equations are:

$$\frac{\partial u_j}{\partial t} + u_j \frac{\partial u_j}{\partial x} + v_j \frac{\partial u_j}{\partial y} = fv_j - g \sum_{i=1}^{n} \frac{\partial h_i}{\partial x} - g \frac{\partial D}{\partial x} + g \sum_{i=1}^{j-1} \varepsilon_{ij} \frac{\partial h_i}{\partial x} + \left(\tau_j^{Tx} - \tau_j^{Bx}\right)/\rho h_j + A \left(\frac{\partial^2 u_j}{\partial x^2} + \frac{\partial^2 u_j}{\partial y^2}\right) \quad (1)$$

$$\frac{\partial v_j}{\partial t} + u_j \frac{\partial v_j}{\partial x} + v_j \frac{\partial v_j}{\partial y} = fu_j - g \sum_{i=1}^{n} \frac{\partial h_i}{\partial y} - g \frac{\partial D}{\partial y} + g \sum_{i=1}^{j-1} \varepsilon_{ij} \frac{\partial h_i}{\partial y} + \left(\tau_j^{Ty} - \tau_j^{By}\right)/\rho h_j + A \left(\frac{\partial^2 v_j}{\partial y^2} + \frac{\partial^2 v_j}{\partial y^2}\right) \quad (2)$$

$$\frac{\partial h_j}{\partial t} + \frac{\partial}{\partial x}\left(u_j h_j\right) + \frac{\partial}{\partial y}\left(v_j h_j\right) = 0 \quad (3)$$

$$j = 1(1)n$$

Where

$$j = 1(1)n$$

Where

n = number of layers

$\varepsilon_{ij} = (\rho_j - \rho_i)/\rho_j$,